Chapter 2

Symmetry Analysis

Symmetries determine several important properties of the studied system, they also influence the experimental outcome. In theoretical physics, a proper understanding of the symmetry of the problem considerably reduces the effort to obtain a desired result. For example, a simple symmetry consideration can provide us with the information that two particular quantities are mathematically equivalent, or that a particular value must vanish. Trying to calculate these values without the knowledge obtained from the symmetry analysis one may end up in an unnecessary consumption of the time and effort, or may even prove impossible.

In solid state physics, the symmetries play an especially important role. It is the translational symmetry which allows for a distinction of solids from molecules, for introduction of the reciprocal space and the existence of the band structure. On the other hand, point group symmetries make the difference between molecules and solids on one side, and free atoms and ions on the other.

One determines the symmetry only with respect to an aspect of the investigated object. In the case of this work, we will investigate symmetries of atomic arrangements (along with their magnetic moments) from the geometric and magnetic point of view, while the nuclear forces acting on elementary particles in our systems are not of our interest. For a symmetry to show up, two conditions must be fulfilled [26]:

- An operation, capable of changing the investigated aspect, must be possible to conduct.

- If this operation leaves the investigated aspect of the system invariant, it belongs to the symmetries of the system.

The first point indicates that for a given system under investigation, a reference system must be present which *will not* be immune to the change. In our analysis, such a reference will be the coordinate system in which we describe the surfaces of the crystals. As a consequence, there is no use in investigating, for example, the magnetization-reversal symmetry of paramagnetic systems.

2.1 State of the Art

The first theoretical explanation of *linear* magneto-optic effects in bulk ferromagnets has been given by Argyres [27] in the 50s. He used linear response theory for current-current correlation functions. His microscopic explanation was already based on the combination of spin-orbit and exchange coupling. The application of linear magneto-optics to antiferromagnetism, however, is unsuccessful in all practical cases. An early theoretical work, based on group-theoretical classification, proposed the use of linear optical effects, namely gyrotropic birefringence, for the observation of AF domains related to each other by the space-inversion operation [28]. A theoretical review of the effects found by a group-theoretical approach is presented by Eremenko and Kharchenko [29]. They performed a comprehensive study of linear optical effects for various AF materials. Another effect proposed recently by Dzyaloshinskii *et. al.* [30] gives a possibility to detect antiferromagnetism taking advantage from optical path differences from antiferromagnetically coupled but intrinsically ferromagnetic planes, e. g. at (111) surfaces of cubic antiferromagnets.

The literature for *nonlinear* magnetooptics is very rich, both in its theoretical and experimental aspect. However, the applications of nonlinear magnetooptics to antiferromagnetism have not been that numerous so far. One of the first theoretical investigations of the possibility to apply nonlinear optics to *antiferromagnetism* was performed by Kielich and Zawodny [31]. These authors predicted, among other effects, the capability of SHG to determine the crystal structure [25].

The first experimental investigation of SHG from antiferromagnetic oxides was the observation of bulk domains in Cr_2O_3 by the Fröhlich group [5]. They observed that circularly polarized light is absorbed differently in two possible domains depending on the handedness of the polarization. Thus, σ^+ light creates SHG mostly in one of the two antiferromagnetic 180° domains, while σ^- light yields SHG response mostly from the other one. Thus a very pronounced intensity contrast of two AF domains is observed in SHG. The authors attributed this contrast to the interference of magnetic and electric dipole contributions, the latter being present only below the Néel temperature. These contributions are described by the nonlinear magnetic and electric susceptibility tensors, denoted as $\chi_m(i)$ and $\chi_e(c)$ respectively. The interference between the two contributions is constructive in one domain and destructive in the other one (for the given helicity of the light), which reflects the fact that $\chi_e(c)$ changes the sign under spin reversal[6] (the operation which leads the domains into each other) while $\chi_m(i)$ remains constant.

From the theoretical point of view, in most cases a symmetry analysis has been applied to study the nonlinear magneto-optical susceptibility tensor $\chi_{el}^{(2\omega)}$ (the source for SHG within the electric dipole approximation). A classification following this approach, with tensors of a rank up to six, has been performed by Lyubchanskii *et al.* [16, 32, 33, 34, 35]. In Ref. [16] the authors include the magnetization-gradient terms and apply the group-theoretical classification to higher-rank susceptibility tensors. This approach then

[6] Originally, the authors use the name "time-reversal", marking by (i) tensors which are invariant, and by (c) those which change sign under this operation. In our opinion the idea of time-reversal cannot be applied to nonlinear optics, thus we use the notion of "spin-reversal". These issues are discussed in detail in Sec. 2.4

allows them to consider the thickness and the character (Bloch vs. Néel type) of domain walls. An attempt by Muthukumar *et. al.* [36] to calculate the $\chi_{el}^{(2\omega)}$ tensor elements for antiferromagnetic Cr_2O_3 both from group theory as well as *from the microscopic point of view* is rather unique. They implemented a $(CrO_6)_2$ cluster, thus taking into account only half of the spins present in the elementary magnetic cell. In this approximation they explained the SHG from Cr_2O_3 as observed by Fiebig *et al.* [5] and they were able to give a quantitative estimate for that. Tanabe *et al.* [37], however, pointed out that the occurrence of purely real or imaginary values of the tensor elements plays a decisive role for the existence of SHG from this substance. They found that for a $(CrO_6)_2$ cluster SHG can take place only in the case where the tensor elements are imaginary, and thus should vanish in Muthukumar's approximation. They proposed to take into account the full unit cell with four inequivalent Cr ions including their "twisting" interaction with the environment. However Tanabe *et al.* neglected the dissipation in the process of SHG[7], which is a rather crude approximation, in particular close to resonances. In general, dissipation makes the $\chi_{el}^{(2\omega)}$ tensor elements complex and invalidates their separation in purely real and imaginary ones [39].

Lifting the inversion symmetry of a crystal is the source for SHG within the electric dipole approximation. Lyubchanskii *et al.* [32, 34] suggested crystal lattice deformations and displacements as possible reasons for SHG from YIG films. In the case of Cr_2O_3 and $YBa_2Cu_3O_{6+\delta}$, described by Lyubchanskii *et al.* [33, 34], AF ordering lowers the symmetry of an otherwise centrosymmetric crystal. In this work, however, we rely on the idea that, rather than lowering the crystal symmetry in the bulk, SHG may also result from the breaking of inversion symmetry at the surface of a bulk inversion-symmetric system. In the next section, we will present our theory for the symmetry analysis of SHG, along these lines.

2.2 Basic Principles of the Symmetry Analysis

In this section, we outline the method to classify the nonlinear magneto-optical response from the symmetry point of view. This presentation will be done in two steps.

- Firstly, we will explain how the symmetries of the sample determine the presence or absence of the elements of the nonlinear optical susceptibility tensor, which is the source of SHG.

- Secondly, we will examine the dependence of these tensor elements on domain operations and the magnetic order parameter. The fact that some tensor elements preserve their sign while others change it under the change of the order parameter is very important for domain imaging.

[7]The authors perform the analysis of $\chi^{(2\omega)}$ in the frequency space. There are no reasons to neglect the damping in this approach. Moreover, if the dissipation is neglected, and $\chi_{ijk}^{(2\omega)}$ is taken as purely real or imaginary, then the Kramers-Kronig relations cannot be applied. In real time, on the other hand, dissipation does not take place, as stated in [38]. This topic will be analyzed more deeply in Sec. 2.4.

The surfaces of NiO serve as an example and guideline for our analysis. In Sec. 2.3, the results of this analysis are applied to particular magnetic systems.

2.2.1 Nonvanishing Tensor Elements

Based on group theory, Dähn *et al.* [40] proposed a new nonlinear magneto-optic Kerr effect (NOLIMOKE) at the (001), (110), or (111) monolayers of cubic antiferromagnets. They also gave an example of an antiferromagnetic structure (the (001) surface of NiO) and an optical configuration, where this new effect could be observed in SHG. Here, we perform a complete group-theory based analysis of collinear AF fcc low-index crystal surfaces. Surfaces of other crystal structures are as well described by our theory provided they are similar to these fcc crystal surfaces, i.e. squares or hexagons. The results can be used to detect the magnetic phase of a specific surface under investigation (to decide if the surface is para-, ferro-, or antiferromagnetic) and allow for the determination of the surface spin configuration in some important cases. However, in order to calculate the SHG yield quantitatively, it is necessary to go beyond group theory and use electronic calculations[8] of the nonlinear susceptibility. Such a calculation will be presented in Chapter 3 of this thesis.

In order to be clear with respect to the essential notion of time reversal we would like to emphasize the point of view taken in this paper in the beginning. Here, we do not divide $\chi_{el}^{(2\omega)}$ into even and odd parts in the magnetic order parameter. Instead, the behavior of $\chi_{el}^{(2\omega)}$ with respect to the magnetic order parameter (which for ferromagnetic materials corresponds to the dependence of $\chi_{el}^{(2\omega)}$ on magnetization) is fully taken into account by the consideration of the magnetic point group. At no stage of our consideration we invoke the notion of time reversal, consequently we do not apply the characterization of the susceptibility $\chi^{(2\omega)}$ as c-tensor (changing its sign under time reversal) or i-tensor (invariant under the time-reversal operation) [39].

Before we start our group theoretical classification of the nonlinear optical susceptibilities of antiferromagnetic (AF) surfaces we would like to emphasize the following four important points:
(i) We are not interested in effects resulting from the *optical path difference* from adjacent crystal planes which are ferromagnetically ordered but only antiferromagnetically coupled to each other. We do not consider this as an intrinsic AF effect.
(ii) Cubic crystals that we are interested in reveal a center of inversion in the para-, ferro-, and all antiferromagnetic phases. Thus, within the electric dipole approximation, the SHG signal exclusively results from the surface.
(iii) While in principle linear optical methods can be sensitive to the presence of a spin structure, in practice they are not useful because, within the group theoretical approach, they cannot distinguish the AF phase from either the paramagnetic or the ferromagnetic one, nor can they distinguish different AF configurations from each other. They have to resort to methods like lineshape analysis, where no strong statements characteristic for symmetry analysis can be made.

[8] Such a calculation necessarily exploits group theory, however.

(iv) Although the tensor elements for all the magnetic point groups are known and tabulated in the literature (e.g. [41]), the connection between the different spin configurations described by us and the mentioned symmetry groups has not been made, except for some easy cases [40]. Thus, for SHG from antiferromagnetic surfaces, there has been up to now no connection at all between the group theoretical classification and the real situations found in experiments on oxide surfaces.

The following part of the text explains the fundamentals of applying NOLIMOKE observations to investigate antiferromagnetism of surfaces.

Now we turn to SHG, the source of which is the nonlinear electrical polarization $P_{el}^{(2\omega)}$ given by:

$$P_{el}^{(2\omega)} = \epsilon_0 \chi_{el}^{(2\omega)} : E^{(\omega)} E^{(\omega)}. \tag{2.1}$$

Here, $E^{(\omega)}$ is the electric field of the incident light, while $\chi_{el}^{(2\omega)}$ denotes the nonlinear susceptibility within the electric dipole approximation, and ϵ_0 is the vacuum permittivity. The intensity of the outgoing SHG light is [42]:

$$I^{(2\omega)} \sim (I_0)^2 \left[\begin{pmatrix} A_1(\Theta)\cos\Phi \\ A_2(\Theta)\sin\Phi \\ A_3(\Theta)\cos\Phi \end{pmatrix} \times \right.$$
$$\times \begin{pmatrix} \chi_{xxx} & \chi_{xyy} & \chi_{xzz} & \chi_{xyz} & \chi_{xzx} & \chi_{xxy} \\ \chi_{yxx} & \chi_{yyy} & \chi_{yzz} & \chi_{yyz} & \chi_{yzx} & \chi_{yxy} \\ \chi_{zxx} & \chi_{zyy} & \chi_{zzz} & \chi_{zyz} & \chi_{zzx} & \chi_{zxy} \end{pmatrix} \times$$
$$\left. \times \begin{pmatrix} B_1(\vartheta)\cos^2\varphi \\ B_2(\vartheta)\sin^2\varphi \\ B_3(\vartheta)\cos^2\varphi \\ B_4(\vartheta)\cos\varphi\,\sin\varphi \\ B_5(\vartheta)\cos^2\varphi \\ B_6(\vartheta)\cos\varphi\,\sin\varphi \end{pmatrix} \right]^2 \tag{2.2}$$

where I_0 is the intensity of the incident light, A_i, B_j ($i = 1..3; j = 1..6$) are Fresnel and geometrical factors for the incident and reflected light, ϑ and Θ angles of incidence and reflection, respectively (ϑ=Θ), and Φ (φ) is the output (input) polarization angle at frequency 2ω (ω). According to Neumann's principle, "any type of symmetry which is exhibited by the crystal is possessed by every physical property of the crystal" [41]. To examine these physical properties, we determine the magnetic point group of the crystal lattice, thus determine its symmetries. The same symmetries must leave the investigated property tensor (in our case the nonlinear electric susceptibility $\chi_{el}^{(2\omega)}$) invariant. This fact is mathematically expressed by the following condition:

$$\chi_{el,i'j'k'}^{(2\omega)} = l_{i'i} l_{j'j} l_{k'k} \chi_{el,ijk}^{(2\omega)}, \quad i,j,k,i',j',k' = x,y,z. \tag{2.3}$$

Here, $l_{n,n'}(n = i, j, k, n' = i', j', k',)$ is a representation of an element of the magnetic point group describing the crystal, i.e. of its symmetry. For symmetry operations including the time reversal there should be an additional "±" sign on the right hand side of Eq.(2.3), but we do not use it here since, as stated before, we exclude the time reversal from our consideration. In particular, from Eq.(2.3) it follows immediately that polar[9] tensors of odd rank (such as $\chi_{el}^{(2\omega)}$) vanish in inversion symmetric structures. This explains why SHG is possible only at surfaces and interfaces, where this symmetry is broken.

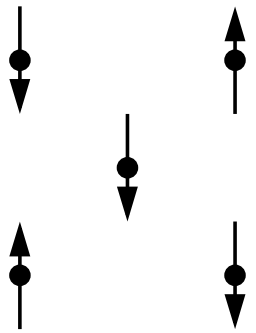

Figure 3: Example of an antiferromagnetic surface spin structure. Arrows represent magnetic moments localized on lattice sites. This fragment, containing 5 lattice sites, fully represents an infinite crystal surface.

For a given spin configuration we apply Eq. (2.3) for every symmetry operation present in the system. Thus, each of these symmetries gives rise to a set of 27 equations with 27 unknown elements of the tensor $\chi_{el}^{(2\omega)}$. This set can be reduced to 18 equations, since

$$\chi_{el,ijk}^{(2\omega)} = \chi_{el,ikj}^{(2\omega)}, \tag{2.4}$$

which expresses the equivalence of the two incident photons of frequency ω in SHG, see also the reduced tensor notation in Eq. (2.2).

As an example, we consider a spin configuration depicted in Fig. 3 which exhibits only one nontrivial symmetry, which is the rotation by 180° degrees around the axis perpendicular to the figure plane (denoted as 2_z). This symmetry operation is represented by the following matrix:

$$l(2_z) = \begin{pmatrix} -1 & 0 & 0 \\ 0 & -1 & 0 \\ 0 & 0 & 1 \end{pmatrix}$$

[9] *Polar* tensors change their sign under the space-inversion operation [41].

Substituting this to Eq. (2.3) one gets the following set of equations:

$$\begin{aligned}
\chi_{xxx} &= -\chi_{xxx} \\
\chi_{xyy} &= -\chi_{xyy} \\
\chi_{xzz} &= -\chi_{xzz} \\
\chi_{xyz} &= \chi_{xyz} \\
\chi_{xzx} &= \chi_{xzx} \\
\chi_{xxy} &= -\chi_{xxy} \\
\chi_{yxx} &= -\chi_{yxx} \\
\chi_{yyy} &= -\chi_{yyy} \\
\chi_{yzz} &= -\chi_{yzz} \\
\chi_{yyz} &= \chi_{yyz} \\
\chi_{yzx} &= \chi_{yzx} \\
\chi_{yxy} &= -\chi_{yxy} \\
\chi_{zxx} &= \chi_{zxx} \\
\chi_{zyy} &= \chi_{zyy} \\
\chi_{zzz} &= \chi_{zzz} \\
\chi_{zyz} &= -\chi_{zyz} \\
\chi_{zzx} &= -\chi_{zzx} \\
\chi_{zxy} &= \chi_{zxy}
\end{aligned} \tag{2.5}$$

Obviously, these equations can be satisfied only if some tensor elements (χ_{xxx}, χ_{xyy}, χ_{xzz}, χ_{xxy}, χ_{yxx}, χ_{yyy}, χ_{yzz}, χ_{yxy}, χ_{zyz}, and χ_{zzx}) vanish. Other tensor elements can have arbitrary values.

Any additional symmetry present in the system will result in a different set of equations which will put additional constraints on tensor elements. We solve the equations for each symmetry separately, since the symmetry operations are independent. In this way, our sets of equations were always limited to 18 equations.

A different symmetry operation than 2_z will result in different constraints. In particular, symmetries whose representations contain off-diagonal matrix elements force some relations between tensor elements in the form of $\chi_{ijk} = \chi_{lmn}$. Generally, if the representation of a symmetry has a complicated form, the set of equations is also complicated. Fortunately, this can always be split into several decoupled subsets. For example, an obvious subset in every case is, due to the existence of the surface, the equation $\chi_{zzz} = \chi_{zzz}$, this tensor element occurs nowhere else. The rank of the other subsets is, as it turns out for our cases, never higher than six. In this manner, one may obtain a set of forbidden elements of the susceptibility tensor as well as relations between allowed ones.

2.2.2 Reversal of the Order Parameter

In the previous subsection we introduced a method which allows to determine the nonvanishing tensor elements (for a given spin configuration). Another interesting issue is the behavior of the tensor elements with respect to the *inversion* or *change* of the AF order parameter **L** (for ferromagnetic phases **L** should be replaced by the magnetization **M**), which is imposed by the operations that transform one domain into another (i.e. domain operations). Let us define the behavior of these tensor elements, which change their sign or are invariant in a given domain operation (which may, but not necessarily does invert the order parameter), as a *domain-parity*. The words "odd" and "even" are used henceforth explicitly with respect to this domain-parity, unless stated differently.

In general, a tensor element can be decomposed in parts odd and even in the domain operation, as shown in Eq. (2.6).

$$\chi_{ijk}^{(2\omega)} = \chi_{ijk}^{(2\omega),odd} + \chi_{ijk}^{(2\omega),even} \tag{2.6}$$

In systems with high symmetry, it is possible to describe an operation which reverses **L** (or **M**) by a spatial operation $\hat{l}$. The operation $\hat{l}$ belongs to the point group of the system, but not to its magnetic point group. The application of this operation to a tensor element will change its sign (keep it invariant) if this element is odd (even) in **L**. Consequently, each tensor element can be either odd or even in **L**, a mixed behavior is forbidden.

Actually, the domain-parity of a given tensor element is a function of the chosen domain operation $\hat{l}$. In most antiferromagnetic configurations more than one operation leading to different domain structures are possible (this means that the order parameter is a vector). For example, for (001) surface one has 4_z rotations (i.e. 90° rotations) leading to different domains *in addition* to the eventual mirror-domain[10] structure. For the (111) surface, there are three domains resulting from the rotations with respect to the z axis alone. For some configurations, they exist in addition to the mirror-domains. The 4_z domain operation, although it does not reverse the order parameter, allows for addressing the domain-parity in a relatively simple way. After applying this operation, a given tensor element is often mapped onto another one[11]. In many cases we were able to detect the change of the sign (or its conservation) under such a mapping, and consequently, in many cases, we give the domain-parity information for tensor elements in the 4_z domain operation. This can ease the analysis of the possible 90° domain imaging on antiferromagnetic surfaces.

Domain structures on (111) surfaces are usually more difficult to address from the point of view of domain-parity. The naive notion of an operation with parity requires that the original situation is restored after applying the operation at most twice. Obviously, 2_z is such an operation and, for certain configurations, 4_z satisfies this criterion as well (where 2_z is just a symmetry operation), besides we were able to draw some conclusions on the domain-parity. However, neither 3_z (120° rotation) nor 6_z (60° rotation) have this property - they must be applied at least 3 times to restore the original situation. Also,

[10] For the definition of mirror domains, see Subsec. 2.3.7.

[11] The indices x and y of the tensor element are exchanged, and a sign change may occur, since $x \to y$ and $y \to -x$.

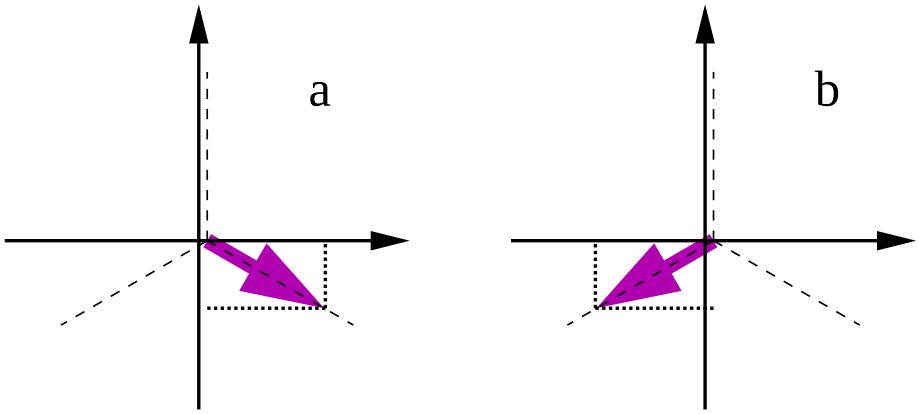

Figure 4: Change of the order parameter (represented by the grey arrow) under operation 3_z. Note that a part of this order parameter changes its sign, while the other remains unchanged.

upon the 3_z operation a single tensor element gets "split" into several tensor elements, and the analysis of the conservation (or not) of the sign of the tensor element looses its sense. The tensor elements are described in the Cartesian coordinate system, where quarters are the elementary entities. Rotation by an angle other than 90° and its multiples cannot be described as interchanging the axes and a possible modification of their signs. However, it is possible to treat the domain-parity of tensor elements in the 3_z and 6_z operation in a more general way. The very fact of having three states prevents us from using the domain-parity in its usual meaning of something simply changing the sign *or* remaining unchanged. Instead, we may allow the domain operation 3_z (for example) to reverse only one part of the order parameter, leaving the other part unchanged (Fig. 4). In other words, we would decompose the order parameter (or an investigated tensor element) into parts whose domain-parity can then be conventionally described. In this way we can deal with the domain-parity of tensor elements on surfaces with arbitrarily complicated domain structure. In this work however, we will not address the domains on (111) surfaces in detail.

In many occasions, it is convenient to define one order parameter that describes equally well all the magnetic phases and spin configurations of a given crystal structure [33, 43]. In this work, we define the order parameters separately for each of the addressed spin configurations[12]. The order parameters defined in this way are, although vectors themselves, components of the order parameter in the sense of [43].

Note, the presence of dissipation (redistribution of response frequencies) does not influence the considerations about the domain-parity. In general, dissipation in frequency space is responsible for the mixing of the real and imaginary parts in the tensor elements (as described in Sec. 2.4), while point-group symmetry governs the (non)existence of tensor elements purely odd or even in the magnetic order parameters **L** or **M**.

[12]For the definition of configurations see Subsec. 2.3.1.

So far we have presented the method used in our symmetry analysis of the surfaces. We know how the symmetries determine the sets of non-vanishing tensor elements and (in some cases) the relations between them. In the next section we will present the results we obtained by applying this method.

2.3 Results of the Group Theoretical Analysis

In the previous section, we presented the method used for the symmetry classification of the surfaces of cubic antiferromagnets. We now apply this method to all distinct spin configurations of low-index surfaces of fcc crystals, including ferro- and paramagnetic surfaces for the sake of completeness. Here, we would like to present the results of this study. This presentation involves:

- nonvanishing tensor elements (and if applicable their domain-parity) for each spin configuration for low index surfaces of fcc crystals,
- influence of different kinds of distortions,
- role of a second layer of atoms,
- conditions for domain imaging,
- considerations about experimental geometries.

The results of the symmetry analysis, presented in this section, can be used in an experiment according to Fig. 5. The detailed description of an experimental use of our results is presented in Subsec. 2.3.8.

2.3.1 "The Table" and How to Read It

The main results of our symmetry analysis is presented in Table I. It displays the nonvanishing tensor elements and the relations between them for each of the spin structures addressed by us. In the current subsection, we explain how this Table should be read. First, we will define the notions of "phase", "case", and "configuration", used henceforth to classify our results.

- "Phase" describes the magnetic phase of the material, i.e. paramagnetic, ferromagnetic, or AF.
- Secondly, the word "configuration" is reserved for the description of the magnetic ordering of the surface. It describes various possibilities of the spin ordering, which are different in the sense of topology. The configurations cannot be transformed into each other by point-group operations, therefore we define the (ferromagnetic or antiferromagnetic) order parameter separately for each configuration. We describe up to 18 AF configurations, denoted by little letters a) to r), as well as several ferromagnetic configurations, denoted as "ferro1", "ferro2", etc. The number of possible configurations varies depending on surface orientation.

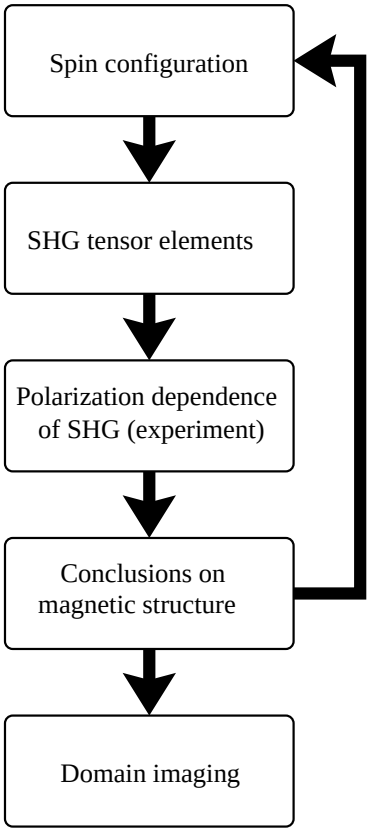

Figure 5: An SHG experiment on an AF surface. Initial assumption about the examined structure is verified by a proper choice of experimental geometry and polarization dependence.

- Thirdly, we describe different "cases", i.e. additional structural features superimposed on the symmetry analysis. "Case A" does not have such additional features - it describes usual surfaces of fcc crystals. In "case B" we address distortions of the lattice of the magnetic atoms. "Case C" deals with two kinds of magnetic atoms in an undistorted lattice. In "case D" we take into account a distorted sublattice of nonmagnetic atoms, keeping the magnetic sublattice undistorted. All the analysis is restricted to collinear antiferromagnets.

The results are displayed by (i) pictures (which define each of the addressed configurations) and (ii) tables (which describe the SHG response of the given configuration).
(i) Presentation in figures. The figures present the spin configurations for the (001), (110), and (111) surfaces. The philosophy of this presentation is that, to avoid extensive length, we show the spin structure in one figure for each surface (Figs. 8, 9, and 10) for all the four cases (A-D), and depict the effects taken into account in the cases B-D only for the paramagnetic phase (Figs. 11, 12, and 13).

Several spin structures depicted in Fig. 8 and Fig. 10 are distinct configurations only in case B, and they are addressed in the tables that concern only this case. For the rest of the cases they are domains of other, fully described configurations, thus they are left out from consideration in these cases.

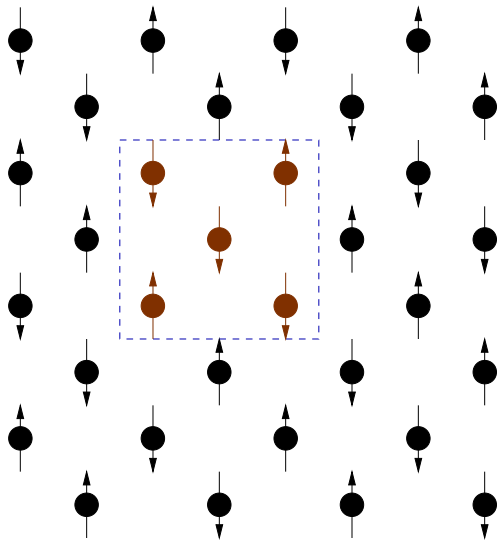

Figure 6: Conventional unit cell as a fragment of an infinite surface.

The figures display "conventional unit cells" with a limited number of lattice sites, however they represent an infinitely extended surface. No oxygen atoms are displayed here. To obtain the whole surface from the depicted fragment, we use the following convention: about the spin structure is presented in Fig. 7 [13]; this neighboring spins along the x and y directions point the same way (alternate) if they are parallel (antiparallel) on the plaquette in these two directions. The spins in rows and columns where only one spin is presented are continued in the same way as the corner spins. This is shown in Fig. 6, for the conf. c) of the (001) surface. This convention will be maintained henceforth (for a (111) surface one has to alter or keep the spins along three axes, instead of two). The smallest set that gives a complete idea "magnetic Wigner-Seitz cell" does not give a clear picture of the crystal symmetries, however. Thus we show the "conventional unit cell" instead (in the sense of crystal lattice theory) as outlined for one example in Fig. 6. The whole crystal lattice can be reproduced by translations of this cell, without performing other operations such as reflections or rotations.

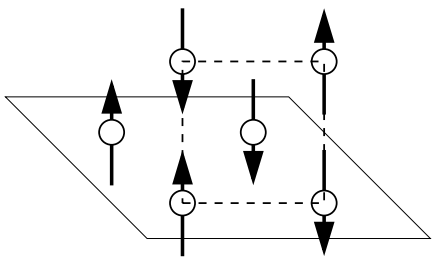

Figure 7: Top view of a spin structure on a (001) surface. The dashed line depicts a conventional unit cell, while the solid one outlines the primitive unit cell.

(ii) Presentation in the tables. First, let us describe briefly the notation[14] used for the symmetry operations. N_i describes a proper rotation, where N is an integer and defines the angle of rotation by $\frac{2\pi}{N}$, and i describes the axis of rotation. The axes are defined in the Figure presenting the corresponding surface. Spatial inversion is described by $\overline{1}$, and combinations of this operation with proper rotations define *improper* rotations, which we

[13] Although our primitive cell contains 4 magnetic atoms they do not fall on a straight line, and thus we still have a two-sublattice antiferromagnet. The primitive cell of a typical four lattice antiferromagnet, like Cr_2O_3 contains 4 magnetic atoms placed on a straight line.

[14] It is commonly called "International Notation".

use describe all the mirror operations in this work. The bar is then put over the multiplicity factor of the rotation.

The tables show the SHG response types for each configuration. The various response types are "encoded" by a "key", which is then "decoded" in Tab. I. This table presents the symmetries, domain operations, and nonvanishing tensor elements for each response type. This is done in order to shorten the overall length of tables, because a given response type can appear in several different cases.

Table I also contains the information on the domain-parity of the nonvanishing tensor elements: the odd ones are printed in boldface. If two or more domain operations have the same effect, we display all of them together. To make the Table I shorter and more easily readable these domain operations (and the corresponding domain-parity information for the tensor elements), that can be created by a superposition of the displayed domain operations, are not displayed. Usually, if more than one domain pattern is possible for a given configuration, the domain-parity of tensor elements is different in different domain operations. For example, if both 90° domains and mirror domains with operation $\overline{2}_x$ are possible, some tensor elements may be, say, odd in 4_z and even in $\overline{2}_x$. This is accounted for by different entries for the domain operations of a given configuration in Table I.

Also, a situation is possible that a tensor element is even in the presented domain operation but is odd in the inverse operation. This fact is expressed by use of italics, and the use of bold- or lightface describes the domain-parity of the tensor element in this operation which is listed in the table. Italic font just hints that the domain-parity changes in the operation which is the inverse of the displayed one. For example, the entry j) of Table I shows a tensor element χ_{xxx} displayed as *xxx*, which is even under the operation 4_z, this means that tensor element χ_{xxx} is odd under -4_z. This behavior of tensor elements may seem strange at first sight. However, it is caused by the fact that under these operations, tensor elements are not mapped on themselves. In our example, after applying 4_z the tensor element χ_{xxx} becomes χ_{yyy}, without changing its sign. If we now apply -4_z, χ_{yyy} (which is under -4_z) becomes χ_{xxx}, again without changing the sign. In order to keep the presentation short, we present the information about the domain-parity of the tensor elements concerning only one domain operation from each pair of mutually inverse operations.

The domain-parity of the elements has been checked in the operations 2_z, 4_z, and in the operation connecting mirror-domains to each other (for the definition of the mirror-domain structure see Subsec. 2.3.7). We do not address the domain-parity of tensor elements in the 6_z nor 3_z operations for (111) surfaces nor any other operation that "splits" tensor elements, although these operations also lead to a domain structure (see Subsec. 2.2.2). As was discussed earlier, it is possible to define a parity of the tensor elements for the 3_z and 6_z operations, however the tensor elements then undergo more complicated changes. The situations where the domain-parity of the tensor elements is too complicated to be displayed in the Table are indicated by a hyphen in the column "domain operation". For some configurations, there is no operation that leads to a domain structure - in those configurations we display the information "one domain".

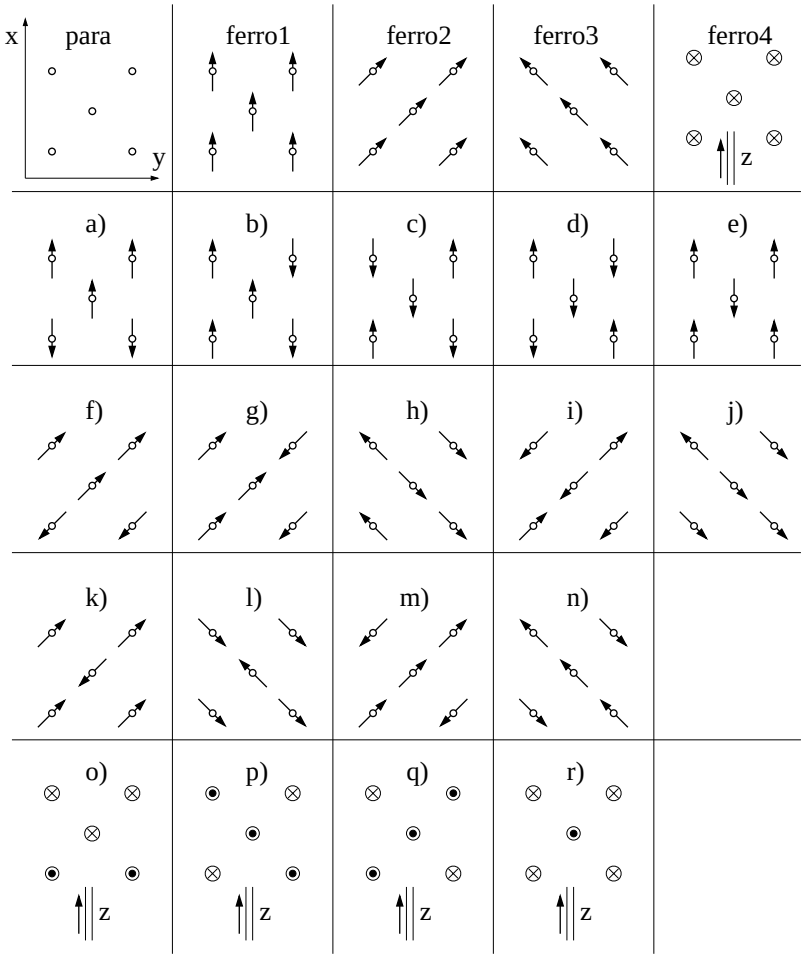

Figure 8: Spin configurations of an fcc (001) surface. Except for confs. "ferro4"and o) - r), the arrows always indicate in-plane directions of the spins. In confs. "ferro4"and o) - r) $\otimes$ ($\odot$) denote spins pointing along the positive (negative) z-direction, respectively.

Scope of the presentation. As far as the first layer is concerned, we address all the collinear spin configurations of the low index surfaces of fcc antiferromagnets, with order parameter **L** lying in plane or perpendicular to it and antiferromagnetic coupling between nearest neighbors. For the (001) surfaces we also discuss the configurations, where the antiferromagnetic coupling exists between the second-nearest neighbors (configurations a), b), c), f), and o), along with d), g), and h) for case B.). We do not consider the coupling to the third and further neighbors. This would not give rise to configurations of different symmetries in two dimensions. It may at most replace spins by grains (blocks) of spins in the configurations described by us. *Thus, our symmetry analysis is complete.*

In this work we thoroughly discuss the spin structure of the first (uppermost) atomic layer. This is sufficient to study all the symmetries of (001) and (110) surfaces both in the paramagnetic and ferromagnetic phases. For the (111) surface it is necessary to recognize the atomic positions (but not the spins) in the second layer for the same purpose. For the sake of completeness we also present a study of (111) surfaces without this extension.

However, in the antiferromagnetic phase, the spin structure of the second and deeper layers plays a role in determining the symmetry of the surface [44]. This is presented in Subsec. 2.3.6, for the simple (undistorted) case, i.e. case A. These structures can serve as simple models for deriving predictions for more complicated cases (B, C, and D), while the full consideration of the second layer would not bring any new interesting results. Taking into account the spin structure of the second layer (deeper layers do not bring up anything new to the analysis) results in creating several (up to two for the (001) surface and three for the (111) surface) configurations out of each one addressed here by us. The symmetry of these configurations may remain the same or be lowered (sometimes even below the symmetry of the ferromagnetic phase) with respect to the "two-dimensional" configurations they are generated from. The results of this analysis are described in Subsec. 2.3.6.

In the next subsections, we will discuss the results of our symmetry analysis.

Table I. Details of SHG response types. We denote $\chi^{(2\omega)}_{ijk}$ by ijk. Odd elements are in bold if a domain operation exists.

key	pt. group	symmetry operations	domain operation	non-vanishing tensor elements
a	4mm	$1, 2_z, \pm4_z, \overline{2}_x, \overline{2}_y, \overline{2}_{xy}, \overline{2}_{-xy}$	one domain	xxz = xzx = yyz = yzy, zxx = zyy, zzz
b	m	$1, \overline{2}_x$	$2_z, \overline{2}_y$	xzx = xxz, **xxy** = **xyx**, **yxx**, **yyy**, **yzz**, yyz = yzy, zxx, zyy, zzz, **zyz** = **zzy**
			$4_z, \overline{2}_{xy}$	no information about the domain-parity
c	m	$1, \overline{2}_{xy}$	$2_z, \overline{2}_{-xy}$	**xxx** = -**yyy**, **xyy** = -**yxx**, **xzz** = -**yzz**, xyz = yxz = xzy = yzx, xxz = xzx = yyz = yzy, **xxy** = -**yyx** = **xyx** = -**yxy**, zxx = zyy, zzz, **zxz** = **zzx** = -**zyz** = -**zzy**, zxy = zyx
			$4_z, \overline{2}_y$	***xxx*** = -*yyy*, xyy = yxx, xzz = -yzz, **xyz** = **xzy** = **yxz** = **yzx**, xxz = xzx = yyz = yzy, *xxy* = -***yyx*** = *xyx* = -***yxy***, zxx = zyy, zzz, ***xzz*** = ***zzx*** = *zyz* = *zzy*, **zxy** = **zyx**
d	4	$1, 2_z, \pm4_z$	$\overline{2}_x, \overline{2}_y, \overline{2}_{xy}, \overline{2}_{-xy}$	**xyz** = **xzy** = -**yxz** = -**yzx**, xzx = xxz = yzy = yyz, zxx = zyy, zzz
e	mm2	$1, 2_z, \overline{2}_x, \overline{2}_y$	$\pm4_z, \overline{2}_{xy}, \overline{2}_{-xy}$	xxz = xzx, yyz = yzy, zxx, zyy, zzz
f	2	$1, 2_z$	$\overline{2}_x, \overline{2}_y$	**xyz** = **xzy**, xxz = xzx, yyz = yzy, **yzx** = **yxz**, zxx, zyy, zzz, **zxy** = **zyx**
			$\pm4_z, \overline{2}_{xy}, \overline{2}_{-xy}$	xyz = xzy, xxz = xzx, yyz = yzy, yzx = yxz, zxx, zyy, zzz, **zxy** = **zyx**
g	mm2	$1, 2_z, \overline{2}_{xy}, \overline{2}_{-xy}$	$\pm4_z, \overline{2}_x, \overline{2}_y$	xxz = xzx = yyz = yzy, **xzy** = **xyz** = **yzx** = **yxz**, zxx = zyy, zzz, **zxy** = **zyx**
h	m	$1, \overline{2}_y$	$2_z, \overline{2}_x$	**xxx**, **xyy**, **xzz**, xxz = xzx, yyz = yzy, **yyx** = **yxy**, zxx, zzz, **zzx** = **zxz**
			$4_z, \overline{2}_{xy}$	xxx, xyy, xzz, xxz = xzx, yyz = yzy, yyx = yxy, zxx, zzz, zzx = zxz
i	1	1	2_z	All the elements are allowed: **xxx**, **xyy**, **xzz**, xyz = xzy, xzx = xxz, **xxy** = **xyx**, **yxx**, **yyy**, **yzz**, yyz = yzy,

key	point group	symmetry operations	domain operation	non-vanishing tensor elements
			$\overline{2}_x$	yzx = yxz, **yxy** = **yyx**, zxx, zyy, zzz, **zyz** = **zzy**, **zzx** = **zxz**, zxy = zyx **xxx**, **xyy**, **xzz**, **xyz** = **xzy**, xzx = xxz, xxy = xyx, yxx, yyy, yzz, yyz = yzy, **yzx** = **yxz**, **yxy** = **yyx**, zxx, zyy, zzz, zyz = zzy, **zzx** = **zxz**, **zxy** = **zyx**
j	m	$1, \overline{2}_{-xy}$	$\pm 4_z, \overline{2}_{xy}, \overline{2}_{-xy}$ $2_z, \overline{2}_{xy}$	no information about the domain-parity **xxx** = **yyy**, **xyy** = **yxx**, **xzz** = **yzz**, xyz = yxz = xzy = yzx, xxz = xzx = yyz = yzy, **xxy** = **yyx** = **xyx** = **yxy**, zxx = zyy, zzz, **zxz** = **zzx** = **zyz** = **zzy**, zxy = zyx
			$4_z, \overline{2}_y$	*xxx* =***yyy***, *xyy* =***yxx***, *xzz* = ***yzz***, **xyz** = **yxz** = **xzy** = **yzx**, xxz = xzx = yyz = yzy, ***xxy*** = ***xyx*** = *yyx* = *yxy*, zxx = zyy, zzz, *zxz* = *zzx* = ***zyz*** = ***zzy***, **zxy** = **zyx**
k	mm2	$1, 2_z, \overline{2}_x, \overline{2}_y$	one domain	xxz = xzx, yyz = yzy, zxx, zyy, zzz
l	m	$1, \overline{2}_x$	$2_z, \overline{2}_y$	xzx = xxz, **xxy** = **xyx**, **yxx**, **yyy**, **yzz**, yyz = yzy, zxx, zyy, zzz, **zyz** = **zzy**
m	1	1	2_z	All the elements are allowed:
			$\overline{2}_x$	**xxx**, **xyy**, **xzz**, xyz = xzy, xzx = xxz, **xxy** = **xyx**, **yxx**, **yyy**, **yzz**, yyz = yzy, yzx = yxz, **yxy** = **yyx**, zxx, zyy, zzz, **zyz** = **zzy**, **zzx** = **zxz**, zxy = zyx **xxx**, **xyy**, **xzz**, **xyz** = **xzy**, xzx = xxz, xxy = xyx, yxx, yyy, yzz, yyz = yzy, **yzx** = **yxz**, **yxy** = **yyx**, zxx, zyy, zzz, zyz = zzy, **zzx** = **zxz**, **zxy** = **zyx**
n	2	$1, 2_z$	$\overline{2}_x, \overline{2}_y$	**xyz** = **xzy**, xxz = xzx, yyz = yzy, **yzx** = **yxz**, zxx, zyy, zzz, **zxy** = **zyx**
o	m	$1, \overline{2}_y$	$2_z, \overline{2}_x$	**xxx**, **xyy**, **xzz**, xxz = xzx, yyz = yzy, **yyx** = **yxy**, zxx, zyy, zzz, **zzx** = **zxz**
p	6mm	$1, 2_z, \pm 3_z, \pm 6_z, 6(\overline{2}_\perp)$	one domain	xxz = xzx = yyz = yzy, zxx = zyy, zzz
q	6	$1, 2_z, \pm 3_z, \pm 6_z$	$\overline{2}_x, \overline{2}_y$	**xyz** = **xzy** = -**yxz** = -**yzx**, xxz = xzx = yyz = yzy, zxx = zyy, zzz
r	3m	$1, \pm 3_z, \overline{2}_y, \overline{2}_{S(xy)}, \overline{2}_{S(-xy)}$	one domain	zxx = zyy, xxz = xzx = yyz = yzy, zzz, xxx = -xyy = -yxy = -yyx
s	1	1	$\overline{2}_y$	All the elements are allowed: xxx, xyy, xzz, **xyz** = **xzy**, xzx = xxz, **xxy** = **xyx**, **yxx**, **yyy**, **yzz**, yyz = yzy, **yzx** = **yxz**, yxy = yyx, zxx, zyy, zzz, **zyz** = **zzy**, zzx = zxz, **zxy** = **zyx**
t	m	$1, \overline{2}_y$	-	xxx, xyy, xzz, xxz = xzx, yyz = yzy, yyx = yxy, zxx, zyy, zzz, zzx = zxz
u	3	$1, \pm 3_z$	$\overline{2}_y$	xxx = -xyy = -yxy = -yyx, **xyz** = **xzy** = -**yxz** = -**yzx**, xzx = xxz = yyz = yzy, **xxy** = **xyx** = **yxx** = -**yyy**, zxx = zyy, zzz
w	1	1	-	All the elements are allowed

2.3.2 Case A: Equivalent Atoms

The predicted new nonlinear magneto-optical effects result from the fact that the magnetic point groups of antiferromagnetic configurations are different from those describing paramagnetic or ferromagnetic phases of the same surface. Since, depending on the magnetic phase, different tensor elements vanish, it is possible to detect antiferromagnetism optically by varying the polarization of the incoming light.

The current subsection discusses nonvanishing elements of the nonlinear susceptibility tensor for an fcc crystal consisting of only one kind of magnetic atoms. The influence of nonmagnetic atoms in the material will be discussed later. The configurations considered here are "ferro1", "ferro2", "ferro4", a), b), c), e), f), i), k), m), o), p), and r) for the (001) surface (see Fig. 8), "ferro1", ferro3", "ferro5", a), c), f), i), and k) for the (111) surface (see Fig. 10), and all configurations depicted in Fig. 9 for the (110) surface. Other depicted spin structures form domains of these configurations and are not referred to in this subsection nor in the tables concerning the current subsection.[15]

configuration	key (response type)
para	a
ferro1	b
ferro2	c
ferro4	d
AF:	
a), b), e), o)	e
c), f)	f
i), k), m), p)	g
r)	a

Table II. SHG response for all spin configurations of the (001) surface of a fcc lattice [45]. For the detailed description of the response types see Tab. I. The configurations are depicted in Fig. 8.

(001) surface. All possible configurations of a fcc (001) surface are shown in Fig. 8. The SHG response types for the (001) monolayer are given in Table II, for the paramagnetic, ferromagnetic, and all AF phases. We can observe several sets of allowed tensor elements. Configuration (conf.) r) will produce the same signal as the paramagnetic phase. Conf. "ferro1" reveals a completely different, distinguishable set of tensor elements. In addition, conf. "ferro2" produces another set of tensor elements, different from any other configuration. It is equivalent to the conf. "ferro1" rotated by 45°. In the confs. a), b), e), and o) we find the same tensor elements as for the paramagnetic phase. However, due to the lower symmetry, their values are no longer related to each other. Confs. c) and f) bring new tensor elements, thus allowing for the distinction of these confs. from the previous ones. Confs. i), k), m), p) reveal the same tensor elements as c) and f) but some of these elements are related. Thus one may possibly distinguish these two sets of configurations. Conf. "ferro4" presents a completely different, distinguishable set of the nonvanishing

configuration	key (response type)
para	k
ferro1	l
ferro2	m
ferro3	n
ferro4	o
AF:	
a), b), c), g) - l)	k
d), e), f)	n

Table III. SHG response for all spin configurations of the (110) surface of a fcc lattice [45]. For the detailed description of the response types see Tab. I. The configurations are depicted in Fig. 9.

[15] If a spin structure is not described within this subsection (nor in the tables relevant to this subsection), it is a domain of the last displayed configuration that precedes the omitted one. This applies to all the Subsections 2.3.2, 2.3.3, 2.3.4, and 2.3.5.

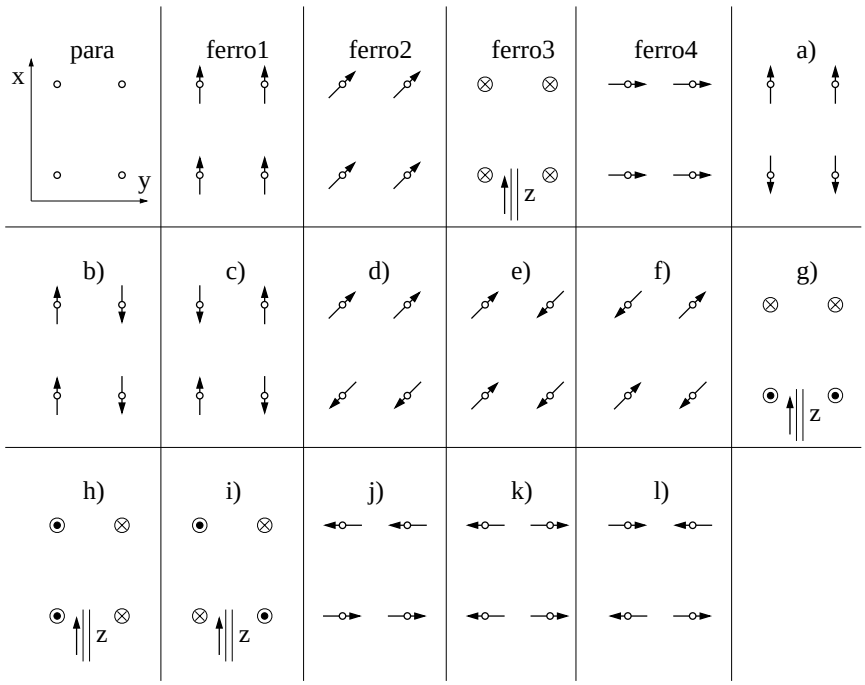

Figure 9: Spin configurations of an fcc (110) surface. Except for confs. "ferro3", g), h), and i), the arrows always indicate in-plane directions of the spins. In confs. "ferro3", g), h), and i) $\otimes$ ($\odot$) denote spins pointing along the positive (negative) z-direction, respectively.

tensor elements. Consequently, in six configurations (i.e. c), f), i), k), m), and p)) some susceptibility tensor elements appear only in the AF phase, allowing for the detection of this magnetic phase by varying the incident light polarization, as will be outlined in Subsec. 2.3.8. In addition, all other antiferromagnetic configurations but r) reveal the breakdown of some of the relations between the different tensor elements, compared to the paramagnetic phase, and thus can be detected as well. Generally, all the magnetic phases can be distinguished from each other. There exists as well the possibility to distinguish different AF configurations provided the corresponding tensor elements can be singled out by the proper choice of the experimental geometry.

(110) surface. We now turn to the (110) surface (Fig. 9), which, in the paramagnetic phase, reveals a lower symmetry than the (001) surface. On the other hand, the number of symmetry operations in the AF configurations is comparable to the (001) surface. In addition, as shown in Table III, the resulting SHG response types are not very characteristic, so the detection possibilities for this surface are very limited. In particular, confs. a), b), c), g), h), i), j), k), and l) give the same tensor elements as the paramagnetic phase. Confs. d), e), f), and "ferro3" bring new tensor elements. Other ferromagnetic configurations ("ferro1" and "ferro2") present different sets of new tensor elements, making these configurations distinguishable from the others as well as from each other. Conf. "ferro4" yields a completely different set of tensor elements, however this set is related to the one of conf. "ferro1" by a 90° rotation.

In short, the (110) surface presents very limited possibilities for any analysis due to a

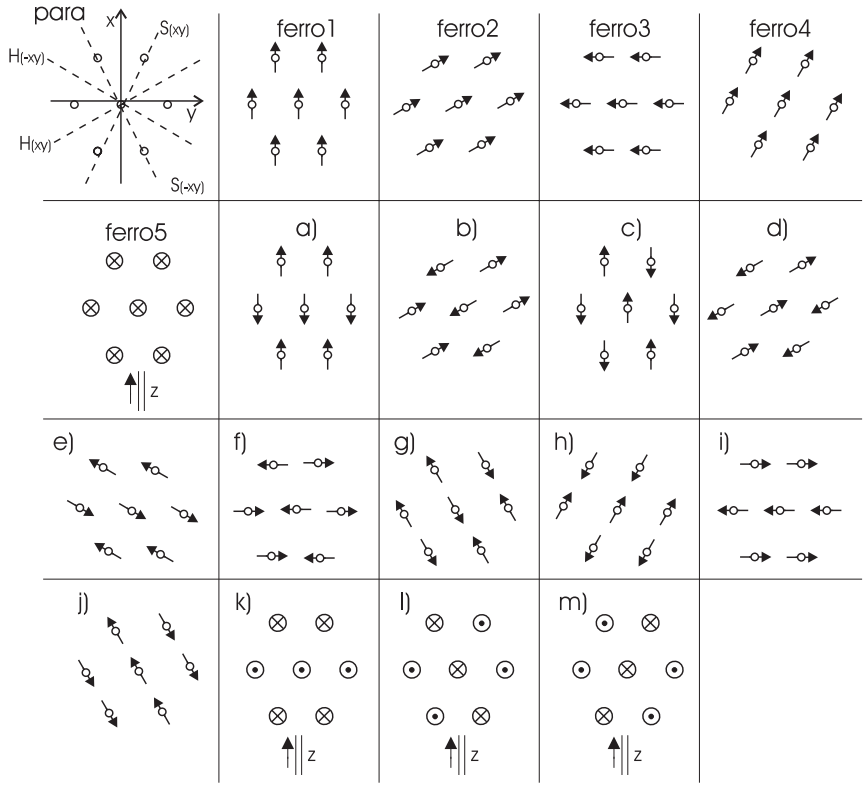

Figure 10: Spin configurations of an fcc (111) surface. Except for confs. "ferro5", k), l), and m), the arrows always indicate in-plane directions of the spins. In confs. "ferro5", k), l), and m) $\otimes$ ($\odot$) denote spins pointing along the positive (negative) z-direction, respectively.

low symmetry already in the paramagnetic phase.

(111) surface. The study of the (111) surface (see Fig. 10) has to be separated in two subcases, according to whether we take into account only one atomic monolayer or more [40]. In both subcases, we consider the same configurations. The SHG response types for the first subcase are listed in Table IV, and for the second subcase in Table V. For the *first* subcase, confs. a), i), and k) reveal the same tensor elements as the paramagnetic phase, however due to the lower symmetry their values are not related to each other. Configurations c) and f) present new tensor elements. As for the previous surfaces, the ferromagnetic phase reveals completely different sets of tensor elements, and the three ferromagnetic configurations can be distinguished from each other since they bring different tensor elements into play. Unlike for the (110) surface, the axes x and y are not topologically equivalent, and thus the fact that tensor elements of "ferro1" are related to those

configuration	key (response type)
para	p
ferro1	l
ferro3	o
ferro5	q
AF:	
a), i), k)	k
c), f)	n

Table IV. SHG response for all spin configurations of the (111) surface of a fcc lattice [45]. Only one monolayer is taken into account. For the detailed description of the response types see Tab. I. The configurations are depicted in Fig. 10.

of "ferro3" by 90° rotation does not affect the possibility to distinguish these two configurations. The ferromagnetic conf. "ferro5" brings up the same tensor elements as AF confs. c) and f), but the relations between the elements are different. The *second* subcase (more layers taken into account) gives different sets of allowed tensor elements (compared to the first subcase) for each but the "ferro3" configuration. Confs. a), i), k), and "ferro3" share the same set of allowed tensor elements and can be easily distinguished from the paramagnetic phase. Confs. c), f), and "ferro1" reveal all tensor elements, with their values unrelated. Similarly, conf. "ferro5" presents another, distinguishable set of tensor elements. The (111) surface presents less possibilities for distinction of the magnetic phases than the (001) surface, but there exist a certain possibility to distinguish the particular AF spin configurations, once the magnetic phase of the material is known.

The symmetry analysis of nonvanishing tensor elements for ferromagnetic surfaces in the case A has been performed by Pan *et. al.* [12]. Our analysis yields the same results, taking into account the corrections made by Hübner and Bennemann [46].

From the above discussion we can state that clearly the best possibilities to distinguish the magnetic phases and spin structures by SHG are presented by the (001) surface. There, the magnetic spin structure of NiO surface - its magnetic phase as well as the particular spin configuration - can be detected unambiguously.

configuration	key (response type)
para	r
ferro1	s
ferro3	t
ferro5	u
AF:	
a), i), k)	t
c), f)	u

Table V. SHG response for all spin configurations of the (111) surface of a fcc lattice [45]. More monolayers are taken into account. For the detailed description of the response types see Tab. I. The configurations are depicted in Fig. 10.

In brief,

- the (001) surface offers good possibilities to distinguish the magnetic phases as well as the particular spin configurations,
- the (110) surface presents poor possibilities for the analysis,
- the (111) surface presents good possibilities for the distinction of the spin configurations, once the magnetic phase of the surface is known.

This concludes the discussion of the simple, undistorted antiferromagnetic surfaces. In the next subsection, we will investigate the influence of the rhombohedral distortion of the lattice.

2.3.3 Case B: Distortions of Monoatomic Lattice

configuration	key (response type)
para	k
ferro1	m
ferro2	o
ferro3	l
ferro4	n
AF:	
a), b) - h), o)	n
i) - n), p) - r)	k

Table VI. SHG response for all spin configurations of the (001) surface of a fcc lattice, distorted to a rhombohedral structure. For the detailed description of the response types see Tab. I. For the surface structure see Fig. 11, for the spin configurations see Fig. 8.

The rhombohedral distortion of the atomic lattice, described here and shown in Fig. 11, makes the x and y axes of the (001) surface inequivalent, even in the paramagnetic phase. On the (111) surface, the y axis is not equivalent any longer to other axes connecting the nearest neighbors. These inequivalences of axes are the reasons for the reduction of the number of symmetry operations already in the paramagnetic phase. Because of this reduction some spin structures that previously formed different domains of a single configuration now cannot be transformed into each other and become "independent"configurations. This happens for almost every of the previously addressed configurations of the (001) and (111) surfaces. Consequently, all the depicted spin structures are in fact configurations, and are addressed in this subsection.

(001) surface. The resulting SHG response types for the (001) surface are listed in Table VI. For this surface, only two of the ferromagnetic configurations, namely "ferro1" and "ferro2" can be easily distinguished from both the paramagnetic as well as the antiferromagnetic phases. These ferromagnetic configurations can also be distinguished from each other. On the contrary, all the AF configurations yield only two types of response, and in addition one of them is equivalent to the response of the paramagnetic phase. Consequently, it will not be possible to determine the surface spin structure, and the distinction of the AF phase from the paramagnetic one can be successfully performed only in confs. a)-h) and o). Compared to the case A, there is an important symmetry breaking for most configurations. Thus, the distinction between the two cases (A and B) is possible (compare Tabs. II and VI).

(110) surface. All the (110) surfaces of an fcc crystal with a rhombohedral distortion are

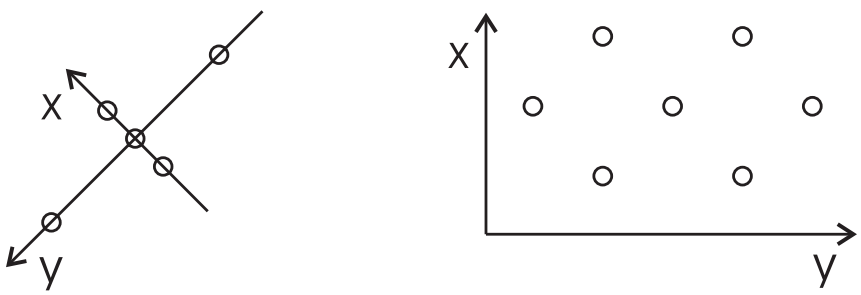

Figure 11: Structure of the (001) and (111) surfaces of a fcc crystal with a rhombohedral distortion in the paramagnetic phase. Note the changed orientation of the coordinate system for the (001) surface.

topographically equivalent to the (110) surface of the case A. The distortion only stretches the x or y axis, so the structure remains rectangular.

(111) surface. The analysis of the (111) surface (also depicted in Fig. 11 in the paramagnetic phase) in the subcase of only one monolayer reveals sets of symmetries very similar to the (110) surface, as it follows from the Table VII. In fact, the (111) surface of a fcc crystal with a rhombohedral distortion can be treated as two rectangular lattices superimposed on each other. In turn, due to the distortion, it is no longer convenient to describe the spin structures using "S"and "H"axes. The possibility to distinguish AF configurations is very poor, and two of the AF configurations (a) and k)) yield the same signal as the paramagnetic surface. In confs. b) - j), l), and m) the AF phase can be distinguished from the paramagnetic one, but they give the same signal as conf "ferro5". Conf. "ferro2"can be easily distinguished since it reveals a characteristic set of (all) tensor elements. Confs. "ferro1"and "ferro3"yield different sets of tensor elements, but they are related to each other by a 90° rotation. Most of the configurations allow for the distinction of the cases A and B (compare Tabs. III and VII).

configuration	key (response type)
para	k
ferro1, ferro4	l
ferro2	m
ferro3	o
ferro5	n
AF:	
a), k)	k
b) - j), l), m)	n

Table VII. SHG response for all spin configurations of the (111) surface of a fcc lattice, distorted to a rhombohedral structure. Only one monolayer is taken into account. For the detailed description of the response types see Tab. I. For the surface structure see Fig. 11, for the spin configurations see Fig. 10.

configuration	key (response type)
para	t
ferro1, ferro2, ferro4, ferro5	s
ferro3	t
AF:	
a), i), k)	s
b) - h), j), l), m)	t

Table VIII. SHG response for all spin configurations of the (111) surface of a fcc lattice, distorted to a rhombohedral structure. More monolayers are taken into account. For the detailed description of of the response types see Tab. I. For the surface structure see Fig. 11, for the spin configurations see Fig. 10.

In the subcase of two monolayers of the (111) surface, the symmetry is dramatically reduced (see Tab. VIII). Even in the paramagnetic phase the group of symmetries consists of only one nontrivial operation, and this occurs also in the AF configurations a), i), k), and "ferro3". In all the other configurations all tensor elements are allowed due to the lack of any symmetry. Only confs. paramagnetic and "ferro5"allow for the unambiguous distinction of the cases A and B (compare Tabs. V and VIII). Consequently, this surface is not very useful to an analysis of the magnetic structure, with the exception of stating the distortion itself.

As the conclusion of the case of the distorted sublattice of magnetic atoms, the surfaces give extremely limited possibilities to investigate the magnetic properties, because of the limited symmetry already in the paramagnetic phase. In our further study, we will limit ourselves to lattices of undistorted magnetic atoms.

In brief, if the monoatomic lattice of magnetic atoms is distorted,

- all the surfaces, (001), (110), and (111), present poor possibilities for detection of the magnetic phase and the spin structure,
- the rhombohedral distortion can easily be detected, regardless of the magnetic phase of the material.

2.3.4 Case C: Structure with Nonequivalent Magnetic Atoms

We assume now that not all the magnetic atoms in the cell are equivalent. An example of such a structure is a material composed of two magnetic elements, but also a situation when the magnetic lattice sites are inequivalent due to different bonds to a nonmagnetic sublattice. Distortions of the sublattice of nonmagnetic atoms that preserve the center of twodimensional inversion (in the paramagnetic phase) produce the same effect. Other distortions of the sublattice of nonmagnetic atoms will be discussed in Subsec. 2.3.5. The magnetic moment at the distinguished positions can be changed or not - this does not affect the results obtained by the symmetry analysis. The configurations considered here are "ferro1", "ferro2", "ferro4", a), b), c), e), f), i), k), m), o), p), and r) for the (001) surface (see Fig. 8), "ferro1", ferro3", "ferro5", a), c), f), i), and k) for the (111) surface (see Fig. 10), and all configurations depicted in Fig. 9 for the (110) surface. Other depicted spin structures form domains of these configurations and are not referred to in this subsection nor in the tables concerning the current subsection.

configuration	key (response type)
para	a
ferro1	b
ferro2	vc
ferro4	d
AF:	
a), o)	h
b), e)	b
c)	f
f)	i
i), m), p)	e
k)	j
r)	d

Table IX. SHG response for all spin configurations of the (001) surface of a fcc lattice, with one atom distinguished. For the detailed description of the response types see Tab. I. For the surface arrangement see Fig. 12. For the confs. see Fig. 8.

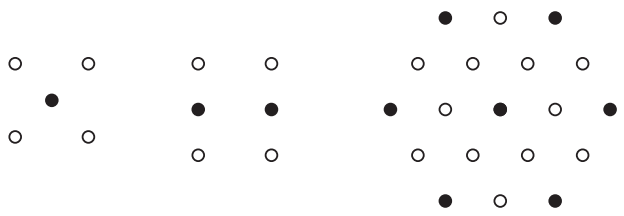

Figure 12: Surface structure of the non-equivalent magnetic atoms case in the paramagnetic phase. Pictures present the (001), (110), and (111) surfaces, respectively. Filled and empty circles represent the two kinds of magnetic atoms. Note, the fragment representing the (111) surface does not show the conventional unit cell but a bigger set of atoms in order to give a clear idea about the surface structure.

The structure is depicted in Fig. 12. For the sake of brevity, we show the structure of the distinguished atoms only for the paramagnetic phase. All the configurations are the

same as in case A, for all surface orientations. The already mentioned "convention" of alternating (or not) spin directions along certain axes is applied regardless of the atom type. This allows us to obtain the whole crystal surface from the small displayed fragment.

(001) surface. Our analysis starts with the (001) surface of an fcc crystal. TheSHG response types for each configuration are listed in Table IX. In general, we can observe seven types of response. The first of them is represented by the paramagnetic phase alone. The second type of response, exhibited by the ferromagnetic "ferro1" and the AF a), b), e), o) confs., differs from any other type by some tensor elements. The confs. a) and o) reveal different tensor elements than the other configurations from the mentioned group. However, the signal from confs. a) and o) is the same as for the confs. b), e), and "ferro1" if one exchanges the axes x and y. Thus, if the directions of the spins cannot be determined by another method, confs. a) and o) cannot be distinguished from b), e), and "ferro1". The next type consists of conf. f) and reveals all tensor elements, while no relations between them are enforced by the symmetry analysis. A completely different type of response is presented by conf. c) alone. Another type, where confs. i), m) and p) belong to brings the same tensor elements as conf. c), but there exist more relations between the elements due to a higher symmetry in these configurations. The next type is given by confs. "ferro2" and k). As in conf. f) all the tensor elements are present but this time there are some relations between them. In addition, confs. r) and "ferro4" yield a completely new set of tensor elements due to the preserved fourfold rotational symmetry.

configuration	key (response type)
para	k
ferro1	l
ferro2	m
ferro3	n
ferro4	o
AF:	
a)	l
b), c), h), i), k), l)	k
d)	1m
e), f), g)	n
j)	o

Table X. SHG response for all spin configurations of the (110) surface of a fcc lattice, with one atom distinguished. For detailed description of response types see Tab. I. For the surface arrangement see Fig. 12. For the confs. see Fig. 9.

Thus, assuming one atom as distinguished may reduce the symmetry. New tensor elements appear in confs. a), b), e), f), k), o), and r) compared to case A (compare Tabs. II and IX). In these configurations it is therefore possible to distinguish the cases of equivalent and nonequivalent magnetic atoms, provided the tensor elements that make the cases different can by singled out by the experimental geometry. There exists also a possibility to distinguish different AF configurations in case C. The antiferromagnetic *phase* can be undoubtely detected in the surface configurations c), f), i), m), and p).

(110) surface. For the (110) surface, there are more possibilities to distinguish the configurations with nonequivalent magnetic atoms than in the case A. However, the configurations still produce ambiguous signals (see Tab. X). Confs. b), c), h), i), k), and l) are equivalent to the paramagnetic phase. Conf. a) is equivalent to the ferromagnetic "ferro1" configuration, and conf. d) to "ferro2". In addition, the confs. e), f), and g) are equivalent to the conf. "ferro3" and conf. j) gives the same signal as conf. "ferro4". Even the presence of nonequivalent atomic sites in the lattice cannot be detected by SHG on

this surface, since the symmetry of the (110) surface is usually not lowered further by the existence of nonequivalent magnetic sites (compare Tables III and X). The only exception are the confs. a), d), g), and j) which give different tensor elements in the two cases. As in the case of equivalent atoms, the (110) surface is not very useful for the analysis.

(111) surface. The study of the (111) surface must again be divided in the two subcases of one or more monolayers, respectively. Fig. 12 depicts the situation in the paramagnetic phase. The SHG response types are listed in Tables XI and XII for the first and the second subcase respectively.
In the first subcase (one monolayer) the symmetry establishes six different types of nonlinear response. The "paramagnetic" type (for the paramagnetic configuration only) is characteristic - all the other configurations have additional tensor elements. The next type of response (the ferromagnetic conf. "ferro1" and the antiferromagnetic conf. a)) brings some new tensor elements. Other tensor elements appear in the conf. k). Configurations "ferro3" and i) show another set of nonvanishing tensor elements. The confs. c) and f) reveal all tensor elements in an unrelated way. In addition, conf. "ferro5" presents a characteristic set of tensor elements.

configuration	key (response type)
para	p
ferro1	l
ferro3	o
ferro5	q
AF:	
a)	l
c), f)	m
i)	o
k)	n

Table XI. SHG response for all spin configurations of the (111) surface of a fcc lattice, with one atom distinguished. Only one monolayer taken into account. For the detailed description of the response types see Tab. I. For the surface arrangement see Fig. 12. For the confs. see Fig. 10.

configuration	key (response type)
para	r
ferro1	s
ferro3	t
ferro5	u
AF:	
a), c), f), k)	s
i)	t

Table XII. SHG response for all spin configurations of the (111) surface of a fcc lattice, with one atom distinguished. More monolayers are taken into account. For the detailed description of the response types see Tab. I. For the surface arrangement see Fig. 12. For the confs. see Fig. 10.

In the second subcase, only four different SHG responses are possible. Firstly, the paramagnetic phase is characteristic - all the other configurations bring additional tensor elements into play. The next type of response is presented by confs. "ferro3" and i) - they yield some additional tensor elements. Confs. "ferro1", a), c), f), and k) reveal all tensor elements and no relations between them appear from our symmetry analysis. Again, the conf. "ferro5" presents a unique set of nonvanishing tensor elements.
Consequently, for the (111) surface, the symmetry breaking due to the presence of a second kind of magnetic atoms has even more important consequences than for the (001) surface. In the situation of only one monolayer, the distinction between the cases may be possible for all the AF configurations (compare Tables III and XI). Considering additional layers leads to further symmetry breaking and renders the distinction between the

configurations impossible. The distinction between the cases A and C is possible in confs. a) and k) (compare Tables V and XII). Besides, in most configurations it is possible to decide if these additional layers play any role (compare Tables XI and XII).

In the Case C, the conditions to distinguish the magnetic structure of the surface are less favorable than in the Case A. The presence of the second kind of atoms reduces the symmetry and can be (in most situations) detected by SHG. Also, one may distinguish AF spin configurations, at least at the (001) surface. In the next Subsection, we will address surfaces where, like in NiO, only one kind of magnetic atoms are present, but the distortion of the oxygen sublattice may result in a different SHG signal.

In brief, if two kinds of magnetic atoms are present (alloying),

- the (001) surface presents good possibilities to distinguish the spin configurations. In some configurations, a possibility to detect the AF phase exists,
- the (110) surface presents poor possibilities to detect of the magnetic structure,
- the (111) surface shows nearly no possibilities to detect of the spin structure, and the SHG signal of the AF phase is the same as for the ferromagnetic phase,
- the presence of the second kind of magnetic atoms can be detected in most situations (except for the (110) surface),
- the presence of the second kind of magnetic atoms slightly reduces the possibilities of detection of the AF phase.

2.3.5 Case D: Distorted Oxygen Sublattice

Due to the strong charge-transfer between nickel and oxygen in NiO the sublattices may be distorted. This effect can lower the symmetry of the surface. A point-charge model calculation by Iguchi and Nakatsugawa [47] presented a shift of the oxygen sublattice ("rumpling") in the direction perpendicular to the surface. Their method did not show any in-plane displacement and thus no change of the surface symmetry. However, if the "rumpling" also has an in-plane component, i.e. if the oxygen atoms are displaced also in the x and y directions, it will also have a considerable effect on the symmetry of the crystal surface. For our analysis, we have chosen a distortion that can lower the symmetry of the surface and besides can be represented within one conventional unit cell. A slight non-stoichiometry of NiO (oxygen vacancies) can produce results qualitatively similar to the ones described in this subsection, however we will not focus on this issue. The configurations considered here are "ferro1", "ferro2", "ferro4", a), b), c), e), f), i), k), m), o), p), and r) for the (001) surface (see Fig. 8), "ferro1", ferro3", "ferro5", a), c), f), i), and k) for the (111) surface (see Fig. 10), and all configurations depicted in Fig. 9 for the (110)

surface. Other depicted spin structures form domains of these configurations and are not referred to in this subsection nor in the tables concerning the current subsection.

As will be shown later, the best conditions for the detection of this kind of distortion are presented by the (110) surface. The (111) surface could show equally good possibilities if only a monolayer of magnetic atoms is present.

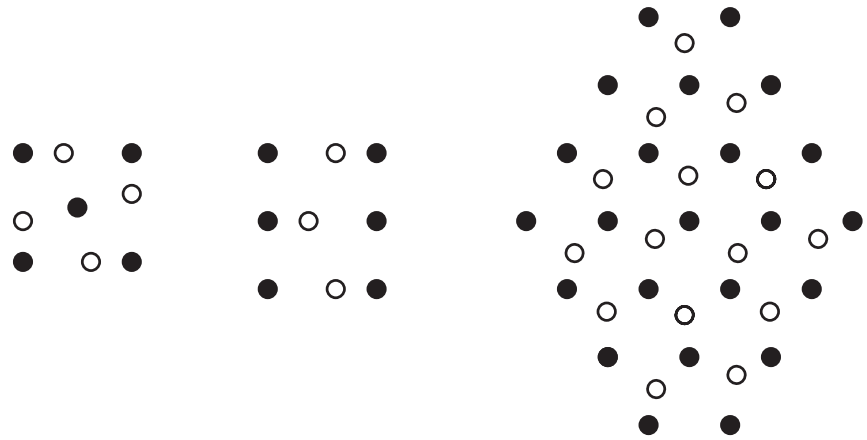

Figure 13: Surface structures of the case with a distorted oxygen sublattice (white circles). Pictures present the paramagnetic phase of (001), (110), and (111) surfaces, respectively. Note, the fragment representing the (111) surface does not show the conventional unit cell but a bigger set of atoms in order to give a clear idea about the surface structure.

In the presence of an oxygen sublattice distortion, the chemical unit cell is also doubled. This effectively means that magnetic unit-cell-doubling (describing the fact that the magnetic unit cell is twice as big as the chemical one) is lifted. In general, taking into account distorted oxygen atoms in the paramagnetic phase does not lower the symmetry of the problem. The exception is the (111) surface, where the six-fold axis is replaced by the three-fold one.

In the case of the distorted oxygen sublattice, the symmetry group for each configuration is a subgroup of the corresponding "non-distorted" configuration, i.e. of the corresponding spin configuration in the case A. As in case C we display only the paramagnetic phase in Fig. 13 to depict the atom positions. All the spin configurations are the same as for the corresponding surfaces in case A, and the spins are assumed to be equivalent.

(001) surface. As Table XIII shows, six different responses can be expected from the (001) surface. The paramagnetic surface will give a characteristic response. The second group is formed by the confs.: a), b), e), o), and "ferro1". Although confs. a) and o) have elements

configuration	key (response type)
para	a
ferro1	b
ferro2	c
ferro4	d
AF:	
a), o)	h
b), e)	b
c), f)	i
i), k)	c
m)	j
p)	e
r)	d

Table XIII. SHG response for all spin configurations of the (001) surface of a fcc lattice, with a distortion of oxygen sublattice. For the detailed description of the response types see Tab. I. For the surface arrangement see Fig. 13. For the confs. see Fig. 8.

different from the remaining configurations in this group, this fact corresponds simply to rotating the sample by 90° with respect to the z axis. Confs. c) and f) reveal all tensor elements without relations between them. Confs. "ferro2", i), k), and m) reveal all tensor elements with some relations. The only difference between conf. m) and others from this group is like for the previous group a 90° rotation with respect to the z axis. Another group consists of conf. p) alone. It reveals the same tensor elements as the paramagnetic phase, but certain relations between tensor elements are broken due to a lower symmetry of the conf. p). The confs. r) and "ferro3" form the last group. All the configurations but k) and "ferro3" can be distinguished from those of case A (compare Tabs. II and XIII). However only confs. c) and g) can be distinguished from case C (compare Tables IX and XIII). Thus, only in these configurations it will be possible to detect oxygen sublattice distortions by SHG.

configuration	key (response type)
para	k
ferro1	l
ferro2	m
ferro3	n
ferro4	o
AF:	
a), b), g), h), k), l)	k
c)	o
d), e), i), j)	n
f)	m

Table XIV. SHG response for all spin configurations of the (110) surface of a fcc lattice, with oxygen sublattice distorted. For the detailed description of the response types see Tab. I. For the surface arrangement see Fig. 13. For the confs. see Fig. 9.

(110) surface. The SHG response types for the (110) surface are presented in Table XIV. One can observe that only configurations c), f) and i) give rise to new (compared to case A, Table II) tensor elements. Compared to case C (Table X), confs. c), f), and i) bring new tensor elements, and, surprisingly, confs. a) and g) have less tensor elements, due to higher symmetries in the case D. Consequently, the confs. a), c), f), g), and i) allow for an unambiguous determination of the oxygen sublattice distortion from the (110) surface. The possibility to distinguish different configurations is rather limited.

(111) surface. Oxygen sublattice distortion similar to the one presented in Fig. 13 for a (111) surface was found by Renaud *et al.* [48] and calculated by Gillan [49] in M_2O_3 materials (M = Al, Fe). Since the nonmagnetic sublattice symmetry group has an influence on SHG this distortion can be detected also on surfaces of fcc crystals. In the previous cases A and C we divided the study of (111) surfaces in two subcases, considering either one or more atomic layers. Taking into account a distorted oxygen sublattice leads us immediately to the subcase of "more atomic layers". It is caused by the fact that, on (111) surfaces, the oxygen and magnetic atoms belong to mutually exclusive planes. The resulting SHG response types are listed in Table XV. For the AF and ferromagnetic phases, all tensor elements are allowed for every configuration. Thus SHG cannot detect the magnetic phase of the surface nor distinguish different configurations. Only confs. paramagnetic, "ferro3",

"ferro5", and d) allow to decide unambiguously whether the oxygen sublattice is distorted or not (compare Tabs. V, XII, and XV).

For both the (001) and (111) surfaces, the symmetry groups of case D appear to be the subgroups of the corresponding configurations of case C. This means that the oxygen sublattice distortion makes some (one half of all) magnetic atoms distinguished as in case C, even though we did not apply this distinction explicitly in case D. On the other hand, the symmetry groups of the case D differ clearly from those of case B. This is caused by the difference in distortions assumed in these cases: the rhombohedral one in case B and rotation-like in case D.

The distortion of the oxygen sublattice diminishes the possibilities to detect the magnetic structure of the surface. Only for the (001) surface one may distinguish the magnetic phases by SHG.

configuration	key (response type)
para	u
ferro1, ferro3	w
ferro5	u
AF:	
All confs.	w

Table XV. SHG response for all spin configurations of the (111) surface of a fcc lattice, with oxygen sublattice distorted. For the detailed description of the response types see Tab. I. For the surface arrangement see Fig. 13. For the confs. see Fig. 10.

In brief, the distortion of the oxygen sublattice[16]

- is possible to detect on (110) and (111) surfaces,
- renders the determination of the spin structure impossible (on all surfaces),
- makes the distinction of the magnetic phases difficult. Only on the (001) surfaces the AF phase can be unambiguously detected.

2.3.6 Second Atomic Layer

In the previous subsections, we took into account the spin structure only for the first (uppermost) atomic layer. For the (111) surfaces, we also addressed the role of the presence (but not the spin structure) of magnetic atoms lying deeper, since this could (and usually did) change the symmetry of the described structure even in the paramagnetic phase. On the other hand, taking into account the positions of the atoms in deeper layers does not change the symmetry for the (001) and (110) surfaces. In this subsection, we present a study of the low index surfaces with more than one layer taken into account, addressing also the spins of the magnetic atoms for the simple (undistorted) case, i.e. case A. The structures described here can serve as simple models for deriving predictions for

[16] Or the mentioned non-stoichiometry.

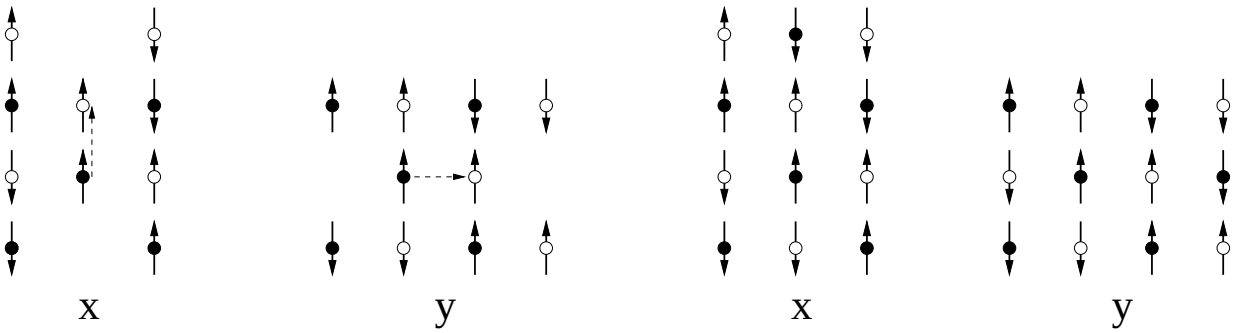

Figure 14: Spin structure of an antiferromagnetic (001) bilayer constructed from a shift of the monolayer along the positive x (y) axis. Filled (empty) circles represent the topmost (second) layer. On the right hand side the conventional unit cells for the resulting bilayer structure are presented. Here, conf. c) of the (001) monolayer serves as an example.

more complicated cases, while the full consideration of the second layer in the other cases (B, C, and D) would not bring any new interesting results. Also, considering more than two layers will not bring any new results, thus our analysis *completely* describes the antiferromagnetic surfaces.

Taking into account the spin structure of the second layer results in creating several (up to two for the (001) surface and three for the (111) surface) configurations out of each one addressed here by us. The symmetry of these configurations may remain the same or be lowered (sometimes even below the symmetry of the ferromagnetic phase) with respect to the "two-dimensional" configurations they are generated from. Consequently the distinction of the configurations from each other may be limited, but the possibility to detect the magnetic phase is not severely affected. Also our remarks on domain imaging remain valid, however the number of domains is increased.

configuration	key (response type)
para	a
ferro1	b
ferro2	c
ferro4	d
AF:	
ax), ox)	h
ay), oy), r)	e
bx), by), ex), ey)	b
c), fx), fy)	i
i)	j
k)	f
m), p)	c

Table XVI. SHG response for all spin configurations of the (001) surface of a fcc lattice, with the spin structure of the second layer taken into account. For the detailed description of the response types see Tab. I. For the confs. see Fig. 8.

(001) surface. The paramagnetic phase and all the ferromagnetic configurations of the (001) surface remain unchanged with respect to the results of the Subsec. 2.3.2 (for the (001) monolayer). However, most of the AF configurations previously addressed break up into two different configurations (sometimes even with a different symmetry). These configurations are constructed from the ones of the previous paragraph by assuming that the structure of the second atomic layer is identical with that of the topmost one but shifted along the positive x axis (indicated by x after the name of the original configuration) or positive y axis (indicated by y after the name of the "parent" configuration) in a proper way to form a fcc structure; if only one configuration can be produced in this way we

use the name of the original one. This construction is depicted in Fig. 14, along with the corresponding conventional unit cells for the two topmost layers of the AF fcc (001) surface. The resulting SHG response types are presented in Table XVI. In general, seven types of response are possible. Firstly, the paramagnetic phase reveals a characteristic set of tensor elements. Thus it can be unambiguously distinguished from any other magnetic phase. Secondly, confs. "ferro1", ax), ox), bx), by), ex), and ey) bring some additional tensor elements into play. The symmetry of confs. ax) and ox) is different from the one of the rest of this group, since the mirror plane is rotated by 90° around the z axis. A different set of tensor elements is brought up by confs. "ferro2", i), m), and p). The difference between the response yielded by conf. i) and the other confs. in this group, due to a different symmetry, can be compensated by rotating the sample by 90° around the z axis. Another, characteristic set of tensor elements is presented by conf. "ferro4"alone. The fifth type of SHG response is given by confs. ay), oy), and r). Tensor elements, that do not vanish in these configurations, are the same as for the paramagnetic phase but some relations between them are broken due to a lower symmetry in the AF phase. Confs. cx), fx), and fy) yield all tensor elements in an unrelated way. The last, characteristic type of response is presented by conf. k) alone. Consequently, the detection possibilities of an antiferromagnetic bilayer are slightly worse than those for a monolayer. Especially, a difficulty in distinguishing the ferromagnetic phase from the antiferromagnetic one may arise for some configurations where then the combination of SHG with other methods is definitely required. There exists a possibility to distinguish AF configurations from each other, similarly to the previous situation. In most configurations, the difference (in terms of the SHG response) between the bilayer structure described here and the previously addressed (001) monolayer can be detected.

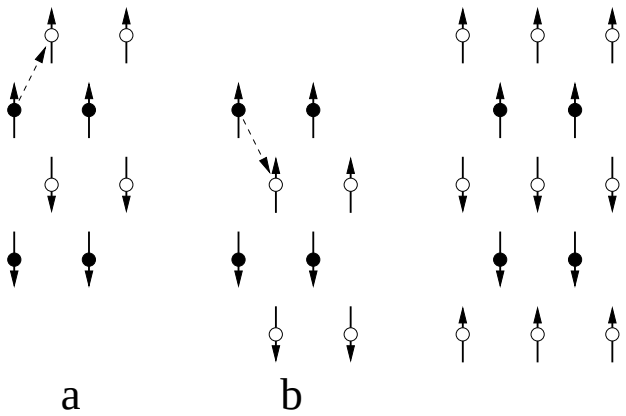

Figure 15: Spin structure of an antiferromagnetic (110) bilayer constructed from a shift of the monolayer, where two different shiftings are applied. Filled (empty) circles represent the topmost (second) layer. The rightmost panel shows the conventional unit cell for the resulting bilayer structure. Here, conf. a) of the (110) surface serves as an example.

(110) surface. The previously described AF configurations of the (001) monolayer most commonly get split into two different configurations when a bilayer structure is considered. For the (110) bilayer it is not the case - only two of twelve AF configurations get split in this way, thus one obtains 14 AF configurations of the (110) bilayer. Describing the results of our analysis we use the nomenclature of our previous article, i.e. the antiferromagnetic configurations are labeled by small letters. Only the four configurations that result from splitting of the two configurations of the monolayer structure are labeled by small letters with subscripts that carry the information about how they have been constructed from the (110) monolayer. For configurations with subscript "a" the lower layer is constructed by translation of the topmost layer by vector (0.5a, 0.5b), where a and b are interatomic

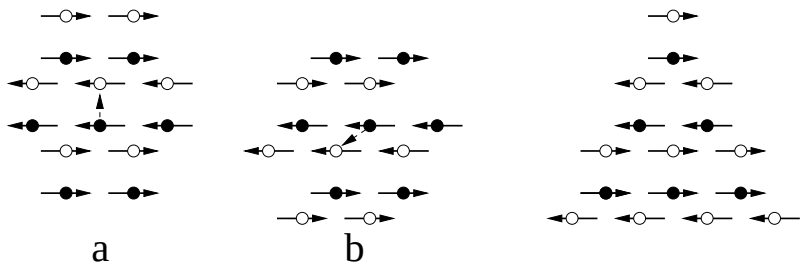

Figure 16: Spin structure of an antiferromagnetic (111) bilayer constructed from a shift of the monolayer, where two different shiftings are applied. Filled (empty) circles represent the topmost (second) layer. Here, conf. f) of the (111) monolayer serves as an example. The rightmost panel displays the conventional unit cell for the resulting bilayer structure of conf. f_a).

distances *within* the (110) plane along x and y axes, respectively. For configurations with subsript "b" the vector of translation is (-0.5a, 0.5b). This corresponds to the way we constructed the (001) bilayers.

The configurations of the (110) monolayer structure are depicted in Fig. 9, and the way the bilayer is constructed is depicted in Fig. 15. The tensor elements are presented in Table XVII. In general, we can observe five types of response. However, the possibility to distinguish AF configurations is not much improved compared to the (110) monolayer. Even the possibility to detect the magnetic phase of the surface is not evident.

As for the (001) surface, there is no difference in SHG signal between the monolayer and bilayer for the paramagnetic and ferromagnetic phases. For most AF configurations, however (confs. a), b), c), e), f_a, f_b), g), h), j), k), and l)) such a difference is present due to a lower symmetry of the bilayer.

configuration	key (response type)
para	k
ferro1	l
ferro2	m
ferro3	n
ferro4	o
AF:	
a), g), j)	o
b), h), k)	l
c), d), l)	n
e), f_a), f_b)	m
i_a), i_b)	k

Table XVII. SHG response for all spin configurations of the (110) surface of a fcc lattice, with the spin structure of the second layer taken into account. For the detailed description of the response types see Tab. I. For the confs. see Fig. 8.

(111) surface. The spin configurations of the (111) bilayer are constructed from the configurations of the (111) surface of our previous work in the way that the spin structure in the second atomic layer is the same as in the topmost layer, but shifted accordingly to

configuration	key (response type)
para	r
ferro1	s
ferro3	t
ferro5	u
AF:	
a_a), a_b), i_a),	
i_b), k_a), k_b)	t
c_a), c_b), f_a), f_b)	s

Table XVIII. SHG response for all spin configurations of the (111) surface of a fcc lattice, with the spin structure of the second layer taken into account. For the detailed description of the response types see Tab. I. For the confs. see Fig. 10.

atoms in the second layer does.

form a hcp structure. Taking into account the spin structure of the second layer causes all the AF configurations to split, thus one obtains 10 AF configurations of the (111) bilayer. The configurations are labeled by small letters (indicating their "parent" configuration) with subscript "a" if the mentioned shifting is along the positive x axis, and "b" if the shifting is along the negative S_{xy} axis.

The configurations of the (111) monolayer are depicted in Fig. 10 and the construction of the bilayer is depicted in Fig. 16. The corresponding tensor elements are displayed in Tab. XVIII. The results are identical to those of the Subsec. 2.3.2, where the second layer of the (111) surface was present but treated as nonmagnetic. This means that the spin structure of the second layer does not play any role for SHG, however the presence of the

In brief,

- (001) surface presents the best possibilities to detect the magnetic phase and the spin structure of the material.
- These possibilities on the (110) surface are limited.
- The results for the (111) surface are the same as in Subsec. 2.3.2.
- In general, the presence of the second atomic layer (and deeper ones) does not invalidate our remarks that SHG is able to detect the magnetic phase and the spin structure of the surface.

2.3.7 Domain Imaging

So far, we have described the possibilities to detect the AF phase and various spin structures on AF surfaces by means of SHG. Another interesting application of SHG is domain imaging in AF materials. As we already pointed out, Fiebig *et al.* [4] were the first to image AF bulk domains in Cr_2O_3. Here, we will analyze the possibilities for the domain imaging on AF *surfaces*.

For simplicity, we will consider here only surfaces described hitherto by the case A of our analysis. In this case, for AF surfaces, no 180° domains can be expected due to the presence of magnetic unit-cell doubling. The allowed domains can be detected by surface-sensitive SHG under the following two conditions.

First, domains can be imaged by our method only if they manifest themselves at the surface, i.e. if the surface spin ordering changes while passing from one domain to another[17]. It is necessary to note, however, that the spin orderings for different domains must belong to the same *configuration* in the sense of our classification. We do not consider it as a domain structure if one portion of the surface is in one configuration and another portion is in a different configuration. Under such conditions, we can encounter two different types of domains: 90° domains (for the (111) surface they are rather 60° domains), resulting from the rotations around the z axis, and the second type (called by us mirror-domains, characteristic for antiferromagnets), where spins point along the same axis in all domains, but the ordering is still different (they are no 180° domains!). The tables contain the complete information about the domain-parity of tensor elements in mirror-domain operations, and also for 90° type domains, but not for 60° domains. The 90° type domains will be addressed later on. In the mirror-domain structure, the magnetic point group describing the configuration must lack an operation that, while belonging to the (nonmagnetic) point group of the system *and* leaving the spin axes invariant, only flips some of the spins. Note, the flipped subset of the spins must be antiferromagnetically ordered in itself. Configurations, the symmetry groups of which *lack* one of these operations can reveal surface domains, related to each other by this operation.

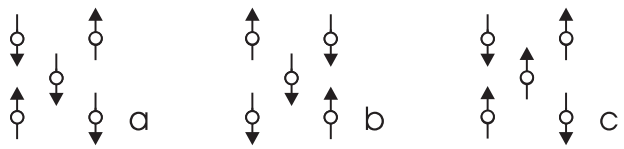

Figure 17: Two surface mirror domains for an AF configuration - panels b) and c) depict the same AF domain, related to the panel a) by different mirror operations.

For an illustration we choose the configuration c) of the (001) surface (see Fig. 8), one of the configurations characteristic for NiO. The spins point along the x axis. Thus operations leaving the axis invariant are $\overline{2}_x$, $\overline{2}_y$ and 2_z. Of them, $\overline{2}_x$ and $\overline{2}_y$ are absent in the magnetic point group of the considered configuration (see Tab. II, conf. c), and Tab. I). The flipped subset of spins consists of the four outer spins for the $\overline{2}_x$ operation, and of the central spin for $\overline{2}_y$ (see Fig. 17 b) and c), respectively). In fact, there are two domains possible in this configuration: one with the spins kept invariant under translations by the vector $(-\frac{a}{2}, \frac{a}{2}, 0)$ (this domain is shown) and the other with the spins kept invariant under translations by the vector $(\frac{a}{2}, \frac{a}{2}, 0)$. Here, a denotes the lattice constant. These domains are depicted in Fig. 17.

The second condition for domain imaging is an interference. It can be created internally by different elements of the tensor $\chi^{(2\omega)}$ or by external reference [50, 51]. The interfering elements should be of a similar magnitude for the largest possible image contrast. Group theory, however cannot account for the amplitudes. With external as well as internal reference, a tensor element that changes its sign under the reversal of the antiferromagnetic order parameter $\mathbf{L}$ is necessary. Actually, every $\mathbf{L}$ dependence of $\chi^{(2\omega)}$ can be represented

[17]It is also possible for different bulk domains to yield the same spin ordering at the surface.

by splitting the tensor elements into odd and even ones in **L**; even if a tensor element is not purely odd or even we can always decompose it according to Eq. (2.6), i.e. a tensor element consists of parts which are odd and even in **L**, respectively. In a system with many terms of that kind the possibility of detecting domains may be limited, since they can influence the signal with opposite sign, thus diminishing the interference. In highly symmetric structures, such as an fcc crystal, the situation is more comfortable: every tensor element is either odd or even in **L** (see Subsec. 2.2.2). By the appropriate set of experiments an element can be singled out and give a clear image of AF domains.

Using our example, conf c) of the (001) surface, we see that in the s-output polarized light only two tensor elements are present[18]: $\chi^{(2\omega)}_{yyz}$ and $\chi^{(2\omega)}_{yzx}$. The first of them is even while the second is odd under the domain operation $\overline{2}_x$. The resulting SHG light I_S can thus be expressed as (compare Eq. (2.2)):

$$I_S \sim (\chi^{(2\omega)}_{yyz})^2 + (\chi^{(2\omega)}_{yzx})^2 \pm 2\chi^{(2\omega)}_{yyz} \cdot \chi^{(2\omega)}_{yzx} \tag{2.7}$$

where "+" stands for one domain, "-" for a different one. The change of sign of one tensor element results in the domain contrast.

Now, we turn to the 90° domain structure. Again, we take the conf. c) of the (001) surface as an example. The operation connecting the domains is 4_z. Under this operation, the tensor element $\chi^{(2\omega)}_{zxy}$ changes its sign, thus again we have an interference which renders the domain imaging possible. This tensor element is even in the domain operation $\overline{2}_{xy}$ (which is equivalent to the superposition of $\overline{2}_x$ and 4_z), which means that domains related to each other by this operation cannot be imaged using this particular tensor element. Similarly, if a tensor element is odd in one domain operation and even in another, it must be odd in their superposition.

It is necessary to mention at this point that taking into account the spin structure in the *second layer* would not change the validity of the analysis presented in this subsection. The only modifications would result from addressing bulk domains rather then surface domains, and the symmetry of the AF configurations would be changed. Yet it would still be possible to find domain operations as well as odd and even tensor elements leading to interference and AF domain contrast. Only in some cases the possibility to identify each of the domains may be limited due to the increased number of domains.

2.3.8 Possible Experimental Results

In this subsection, we propose and discuss possible experimental setups for the detection of AF configuration and the imaging of AF domains from low-index surfaces of NiO that exhibit magnetic unit-cell doubling in contrast to bulk Cr_2O_3 [5, 24]. We propose an experimental setup for the *detection* of antiferromagnetism in the following way: both the incident and reflected beams may lie in the xz plane (optical plane), and form the angle ϑ with the z-axis (normal to the sample surface). In the plane perpendicular to the outgoing

[18]For simplicity, the result of the symmetry analysis of a monolayer (case A) are used here. The tensor elements resulting from a bilayer (Subsec. 2.3.6) do not hamper the possibility of domain imaging, but would make the presentation more cumbersome due to the enhanced number of tensor elements.

beam axis, the electric field of the second-harmonic generated light has two components, $E_p^{(2\omega)}$ and $E_s^{(2\omega)}$, given by the formulae

$$\begin{aligned} |E_p^{(2\omega)}| &= |\cos\vartheta E_x^{(2\omega)} - \sin\vartheta E_z^{(2\omega)}| \\ |E_s^{(2\omega)}| &= |E_y^{(2\omega)}| \end{aligned} \tag{2.8}$$

$E_x^{(2\omega)}$, $E_y^{(2\omega)}$, and $E_z^{(2\omega)}$ are the components of the electric field resulting from SHG in the coordinate system of the sample. The dependence of these components on the input electric field is indicated by the tensor $\chi^{(2\omega)}$. The aim of the experiment is the determination of vanishing and nonvanishing tensor elements. The easiest way to do this is to analyze the output signal intensity as a function of the input polarization in both output polarizations s and p, for a fixed angle of incidence and reflection. The dependence of the output second-harmonic electric field on the input polarization is schematically displayed in Fig. 18 for all tensor elements. The intensity of SHG light is the square of the linear combination of these partial responses. Examples of the intensity dependence on the input polarization is presented in Fig. 19 for all the magnetic phases. The intensity need not be symmetric with respect to $\varphi = 90°$, this results from the influence of the electric field depicted in Fig. 18c). The coefficients of the mentioned combination are the products of the $\chi^{(2\omega)}$ tensor elements and the corresponding Fresnel coefficients, according to Eq. (2.2). Thus performing a best fit of these coefficients to the experimental results will give (after taking into account the Fresnel and geometrical coefficients, known for the given experimental geometry and material [42]) a set of non-vanishing elements of the $\chi^{(2\omega)}$ tensor. Thus for instance, the magnetic phase can be determined.

Concerning another experimental geometry, with input polarization fixed and intensity measured as a function of the output polarization, it is possible to determine whether the nonlinear Kerr effect takes place. For instance, with the input polarization $\varphi = 90°$, the output electric field is given as follows [42]:

$$E^{(2\omega)} = \sin\Phi(A_2(\Theta)\chi_{yyy}^{(2\omega)}B_2(\vartheta)) + \cos\Phi(A_1(\Theta)\chi_{xyy}^{(2\omega)}B_2(\vartheta) + A_3(\Theta)\chi_{zyy}^{(2\omega)}B_2(\vartheta)) \tag{2.9}$$

As the result, maximum of the intensity is for $\Phi \neq 90°$, if at least one of the tensor elements $\chi_{xyy}^{(2\omega)}$ or $\chi_{zyy}^{(2\omega)}$ does not vanish. Actually, tensor element $\chi_{zyy}^{(2\omega)}$ is even in all the investigated order parameters, but the tensor element $\chi_{xyy}^{(2\omega)}$ can be odd. For such configurations the Kerr effect (change of polarization caused by inversion of the magnetic order parameter) takes place. Thus, it is possible to determine which tensor elements are associated with the spin-orbit coupling.

The geometry with p polarization of the reflected SHG light seems to be less useful, since there the tensor element $\chi_{zzz}^{(2\omega)}$ is always present, regardless of the configuration. Besides, this polarization mixes the $\chi_{x..}^{(2\omega)}$ and $\chi_{z..}^{(2\omega)}$ tensor elements. This mixing, however, can be tuned by varying the angle of incidence ϑ and taking into account the influence of the Fresnel coefficients. For smaller ϑ only the $\chi_{x..}^{(2\omega)}$ elements are important, while for larger ϑ the $\chi_{z..}^{(2\omega)}$ dominate. If the experiment does not show any difference for these two situations, the tensor elements must be related. This is the possibility to distinguish the configurations with some relations between the tensor elements from those without such

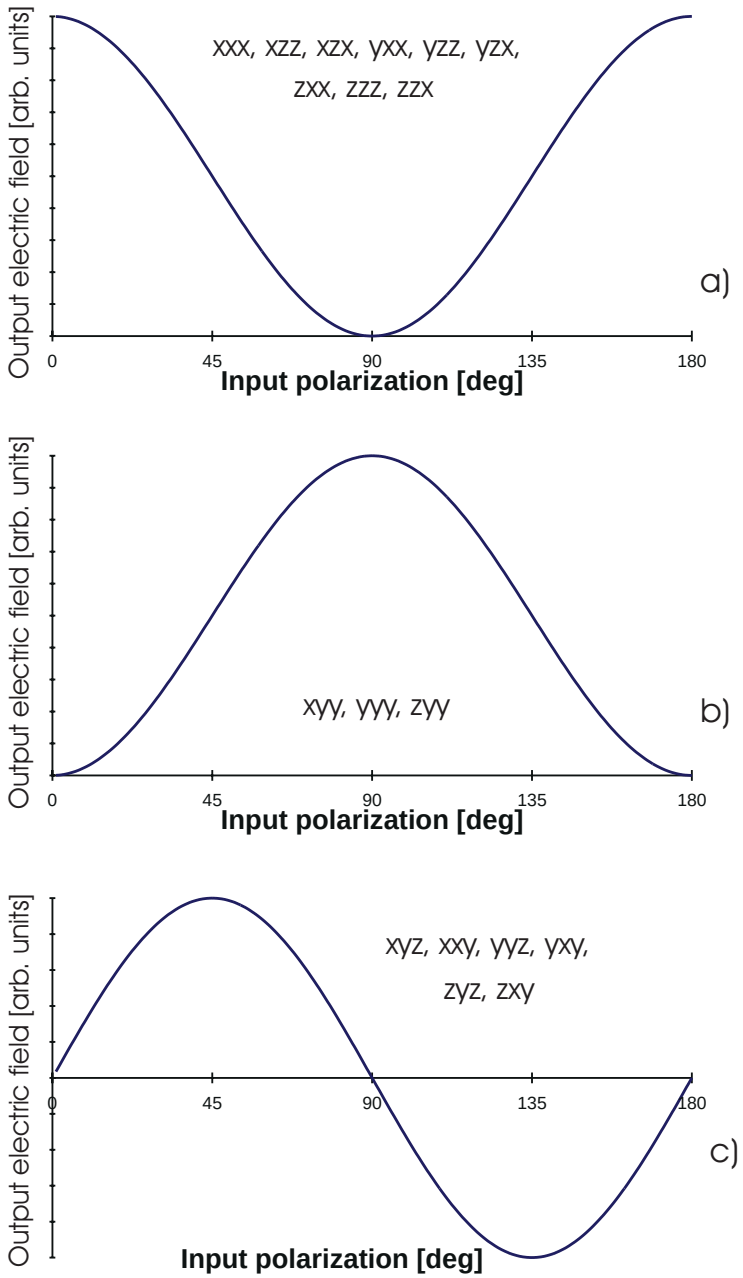

Figure 18: Electric field response of single tensor elements as a function of the input polarization. Tensor element $\chi_{ijk}^{(2\omega)}$ is denoted as ijk.

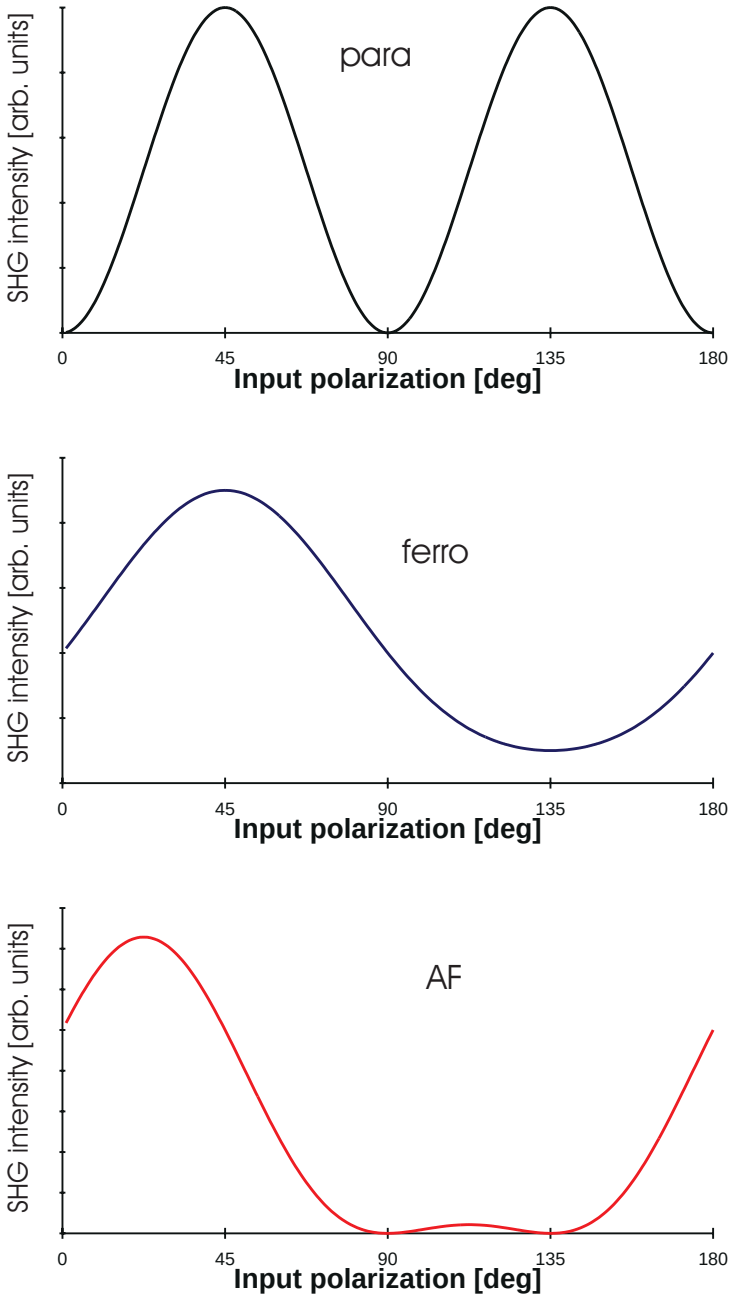

Figure 19: SHG intensity in S-output geometry for different magnetic phases.

relations. On the other hand, the s polarization gives better chances for singling out the desired tensor elements.

The surface, which gives the best possibilities of drawing practical conclusions in an experiment, is the (001) surface. This is true not only for monolayers with an undistorted structure, as described by Dähn *et al.* [40], but also in case of a real surface (as represented by our analysis of a bilayer structure). In particular, Fig. 19 shows the possibility of distinguishing magnetic phases of the (001) surface[19], which, in the case of the structures presumed for NiO, remains valid both for the monolayer and the surface. The most important difference between the paramagnetic and the both magnetically ordered phases is the fourfold symmetry of the SHG response for the first one. Two minima in the response of the AF surface clearly distinguish it from the ferromagnetic phase. In the real experiments, these minima need not be separated by 45°, nor the response needs to fall to zero. Both these features depend on the relative complex phase and magnitude of the tensor elements. As our eletronic calculation in Chapter 3 hints, one can choose such a wavelength that the tensor elements are similar, with respect to the complex phase *and* the magnitude. Thus, one can expect the experimentally obtained polarization dependence of SHG to be similar as in Fig 19c).

In brief, the features of the experimental s-polarized SHG response from the (001) surface are expected to be as follows:

- paramagnetic phase: fourfold symmetry.
- ferromagnetic phase: twofold symmetry, one minimum.
- antiferromagnetic phase: twofold symmetry, two minima.
- domain imaging: both 90° and mirror domains possible to image.

2.4 Time Reversal

As was discussed in the previous sections, symmetries determine the optical response of a crystal. In magnetic materials, time-reversal is believed to be of fundamental importance since this operation reverses all magnetic moments [8, 24, 29]. However, the consequences of applying time-reversal are more profound than a simple inversion of localized magnetic moments. As it will turn out in the current section, there is a deep interrelation between the absence of conventional dissipation in even-order (e.g. second) harmonic generation and the influence of time-reversal on spin ordering. This brings about a subtle difference between time-reversal and spatial symmetries in nonlinear optics. The benefit of this difference makes optical second harmonic generation (SHG) a rather unique probe of antiferromagnetism, while linear optics (where dissipation in the conventional sense is possible) is blind for such balanced spin structures. The recent discussion about the influence

[19]The ferromagnetic configuration "ferro1" and the AF configuration c) were used to obtain the graphs.

of micro-irreversibility on macro-reversibility and reciprocity ([52, 53, 54]) shows that the issue of time-reversal, although extensively discussed, is far from being understood.

In this section, we will:

- present the contemporary status of applying of the time-reversal operation in the symmetry analysis,
- discuss the issue of two kinds of dissipation in nonlinear magneto-optics,
- analyze the reversibility of an elementary process of SHG, and
- propose a novel operation which is better suited for the symmetry analysis of nonlinear magneto-optics.

2.4.1 Conventional Approach

In considering the time-reversibility of an experimental situation, three approaches are possible: (i) time-reversal is applied to the sample, but all the processes resulting from the experiment are unchanged. In particular, the magnetic moments in the sample are reversed, but the direction of the light propagation through the sample is not affected. This approach is presented e.g. in [55, 56]. We consider this approach as incomplete, since it does not equally treat the sample and the light propagating through it. (ii) The second approach, usually encountered in the so called Sagnac-interferometry, addresses time-reversal by reversing the propagation of the light through the sample (see, e.g. [57, 58, 59]). Clearly, such procedure probes the *reciprocity* [60] of the sample rather than its time-reversal symmetry. It can also be proven that the second approach is equivalent to the first one. (iii) According to the third approach, presented e.g. in [61], time reversal acts on *both*: the sample and the experimental setup. In this work, we follow approach (iii).

2.4.2 Dissipation in SHG

In the processes of even-order harmonic generation, dissipation in the conventional sense, converting radiation into heat, does not exist, since the energy loss of the electromagnetic field is the time average [38]

$$-\left\langle \frac{dP(t)}{dt} E(t) \right\rangle, \tag{2.10}$$

which vanishes for SHG (and all even-order harmonics), since

$$\begin{aligned} P(t) &\sim P_0 e^{i\omega t} \\ E(t) &\sim E_0 e^{i2\omega t} \end{aligned} \tag{2.11}$$

Here, P and E denote the polarization of the medium and the electric field, respectively[20]. The lack of dissipation in the conventional sense does not mean that the process of SHG is reversible. Already the analysis by Armstrong *et al.* [62] assumes a unique time direction. There, the nonlinear polarization $\mathbf{P}^{NL}$ and the electric field $\mathbf{E}_3$ of a light beam resulting from Sum Frequency Generation at a point r_0 is given by:

$$\mathbf{P}^{NL}(\omega_3) \sim \frac{1}{2}\mathrm{Re}\left[e^{i(\Delta\mathbf{k}\cdot\mathbf{r_0}+\Delta\phi)}e^{i(\mathbf{k_3}\mathbf{r_0}-\omega_3 t+\phi_3)}\right] \tag{2.12}$$

$$\mathbf{E}_3 \sim \mathrm{Re}\left[e^{i(\mathbf{k_3}\cdot\mathbf{r_0}-\omega_3 t+\phi_3)}\right], \tag{2.13}$$

see eqs. (3.1) and (3.2) of Ref. [62]. Here, ω_3 and k_3 describe the frequency and wave vector of the generated light ($\omega_3 = \omega_1 + \omega_2$ and $\mathbf{k_3} \approx \mathbf{k_1} + \mathbf{k_2}$). The authors introduce the idea of "work done on this wave" by the nonlinear polarization of the medium, equal to

$$W_3 = \frac{\omega_3}{2\pi}\int_{cycle}\mathbf{E}_3\frac{d\mathbf{P}^{NL}(\omega_3)}{dt}dt = \frac{1}{2}\omega_3\mathbf{E}_3\mathbf{P}^{NL}(\omega_3, \text{out-of-phase}), \tag{2.14}$$

if the polarization is exactly 90° out of phase with the electric field (which requires that $\Delta k_z z + \Delta\phi = \pi/2$). The work done on the generated wave *determines the direction of time*. This presents a new kind of dissipation, namely "dissipation in the frequency space", which invalidates time-reversal symmetry.

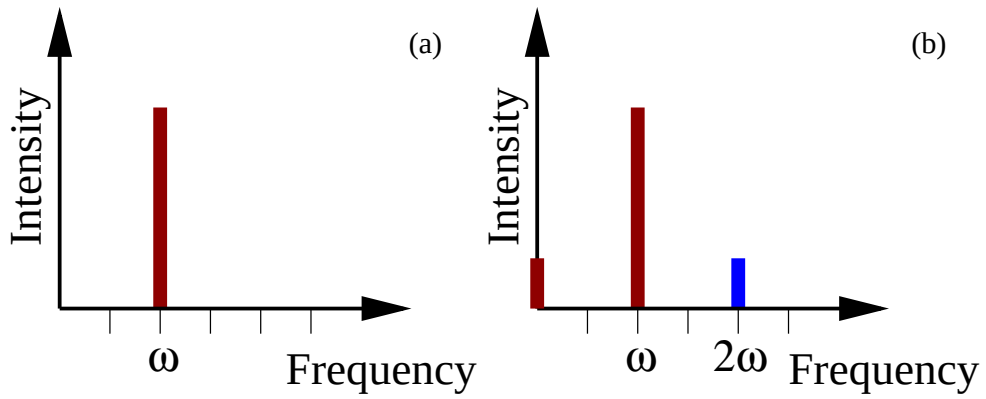

Figure 20: Light intensity distribution on the input (a) and on the output (b) of the SHG.

[20]Both ω and 2ω beams can be attenuated during their propagation, but this is merely dissipation in the linear propagation of the wave through a medium. In our analysis, we neglect this kind of dissipation. Under this condition, linear optics is reversible. This can be seen for example in the Faraday effect, which (in the absence of dissipation) consists only of the rotation of the polarization plane (no induced ellipticity). After applying the time-reversal operation, the polarization of the light at the output (of the reversed process) is the same as the polarization at the input of the original process, thus time-reversal symmetry is preserved. This is true if one follows our convention and applies the time reversal *both* to the sample and to the measurement process.

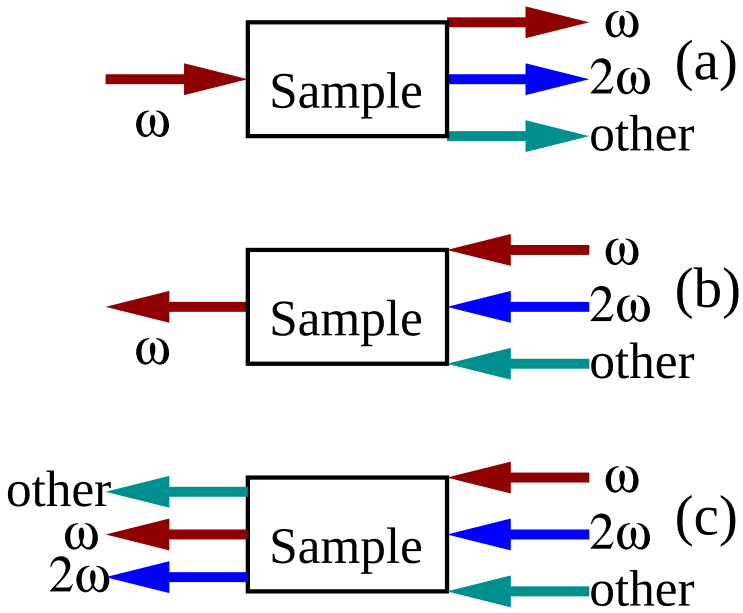

Figure 21: Time-reversal asymmetry in SHG. Panel (a) presents the original process, panel (b) a process in reversed time which would restore the symmetry, panel (c) presents a physically valid process described in reversed time.

As stated before, there is no dissipation in the process of SHG in the usual meaning, i.e. the amount of energy in the radiative form is constant. However, there is a transfer of energy between the frequencies, in particular energy flows from the frequency ω to other frequencies (see Fig. 20). We call this *dissipation in frequency space*, in contrast to the more usual *dissipation in real time*. Dissipation in frequency space can mix real and imaginary parts of the nonlinear susceptibility tensor. The distinction between these two types of dissipation is often encountered in the literature. We consider them here on an equal footing stating that the presence of any of them (in our case it is the dissipation in frequency space) causes the system to have dynamical [63] and thus irreversible properties. In this case, time-reversal does not apply to the symmetry analysis [36, 40, 41].

This fact becomes even more obvious if one takes the global picture of SHG. Radiation acting on an *ensemble of atoms* may excite and deexcite them in many ways *simultaneously*. Thus contributions of many frequencies are always present (see Fig. 21(a)). One has a unique source of ω light but several detectors for beams of different frequencies: 2ω, 3ω, etc, resulting from sum frequency generation (in particular SHG); linearly propagating ω light; and a DC current resulting from difference frequency generation. This is due to the expansion of the source term (polarization $\mathbb{P}$) in terms of the electric field:

$$\mathbb{P} = \mathbf{P_1} + \mathbf{P_2} + \ldots = \chi^{(1)}(\omega)\mathbf{E}^{(\omega)} + \chi^{(2)}(\omega)\colon \mathbf{E}^{(\omega)}\mathbf{E}^{(\omega)} + \ldots \tag{2.15}$$

Imposing time reversal, the detectors become sources and vice versa. Thus, in the time reversed process, one ends up with a single detector, the one which receives the light of frequency ω (Fig. 21(b)). In order to obtain this single frequency one has to redirect all these (previously generated) beams back to the sample, conserving their phase. The source

term now becomes:

$$\mathbb{P} = \chi^{(1)}(\omega)\mathbf{E}^{(\omega)} + \chi^{(1)}(2\omega)\mathbf{E}^{(2\omega)} + \ldots + \chi^{(2)}(\omega)\colon \mathbf{E}^{(\omega)}\mathbf{E}^{(\omega)} + \chi^{(2)}(2\omega)\colon \mathbf{E}^{(2\omega)}\mathbf{E}^{(2\omega)} + \ldots \tag{2.16}$$

Since the phases of the now incident electric fields are the same as for the previously outgoing electric fields, all the terms but those with $\chi^{(1)}$ cancel (which means that in the outgoing light one now has only the contribution at the frequency ω) and the original situation at the input of the process is restored. This description, though mathematically correct, is physically invalid, since there is no practical way to detect an infinite array of frequencies along with the beam phases and to revert it with arbitrary accuracy (Fig. 21(c)). Tracing out the "bath" degrees of freedom (frequencies other than ω and 2ω) causes a transition from a pure to a mixed state of the system, which means that some memory is lost. This happens because the traced subsystem and the bath are not statistically independent [64]. Thus, in any practical situation, there is no possibility to generate only the frequency ω out of a whole array of frequencies. The process of SHG looks different in time t than in the reversed time $-t$. Such a process is called *dynamical*.

2.4.3 Spatial Operations

So far we have reasoned that the time-reversal operation has to be excluded from the symmetry analysis of SHG. However, *magnetism* may bring an additional complication, since the magnetic spin structure is an additional aspect the symmetry analysis must account for, and it is the time-reversal which is conveniently applied to flip the local magnetic moments. This is, however, not correct: it is the classical covering symmetry [65] of the magnetic crystal which should be addressed in a symmetry analysis rather than the quantum-mechanical symmetry of the wavefunctions[21]. This means that the operation applied to reverse the localized magnetic moments should be performed in real space rather than Hilbert spin space. Consequently, time-reversal cannot be used for the symmetry classification of magnetic moments.

Taking into account that time-reversal is not suitable for the description of dynamical phenomena, one needs an operation which merely flips the localized magnetic moments without inverting the time-flow. This can be accomplished by purely spatial point-group operations. In many *antiferromagnetic* (e.g. transition-metal-oxide) crystals a simple translation by a lattice vector reverses the magnetic moments. In many ferromagnetic and antiferromagnetic systems this may be accomplished by a mirror operation. The spatial operation, which reverses the localized magnetic moments, is called by us "moment-reversal". This operation is obviously unitary, in contrast to the time-reversal operation, which is anti-unitary. Consequently, one does not need to invoke the time-reversal operation to describe the full symmetry of magnetic crystals.

[21] According to [65], both the σ_x and σ_y operations cause reversal of the spin part of the quantum-mechanical fermionic wavefunction. Of them, σ_y is conveniently used to describe time-reversal, since it is an anti-unitary operation [66].

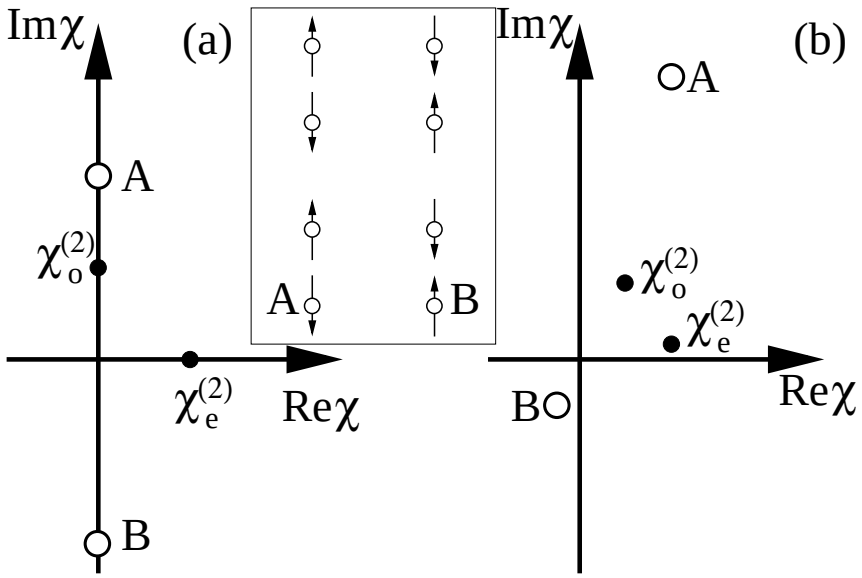

Figure 22: Nonlinear susceptibility tensor elements and resulting SHG intensity using time-reversal (panel (a)) and spin-reversal (panel (b)). Position of the points "A" and "B" is given by $(\chi_e^{(2)})^2 + (\chi_o^{(2)})^2 \pm 2\chi_e^{(2)} \cdot \chi_o^{(2)}$, and the distance of the points "A" and "B" from the origin of the complex plane corresponds to the intensity of SHG from the domains A and B, respectively (see inset for an example of domains in Cr_2O_3). For simplicity, the moduli of the tensor elements have been taken as equal to 1, but the argumentation also holds in the general case.

2.4.4 Practical Implications

Next, we support our reasoning by an example where the application of time-reversal and "moment-reversal" in the symmetry analysis yields different results (see Fig. 22). Let us assume a spin structure with two domains, A and B, related to each other by spin-reversal[22]. A symmetry analysis, similar to the one in [67], provides us with the set of nonvanishing elements of the nonlinear susceptibility tensor (i.e. $\chi^{(2)}$ tensor) along with the parities of these elements. Let us assume that for a certain experimental geometry only two tensor elements, called $\chi_o^{(2)}$ and $\chi_e^{(2)}$, contribute to the resulting SHG light, and that $\chi_o^{(2)}$ is odd while $\chi_e^{(2)}$ is even in the domain operation. The intensity of SHG light at a fixed polarization is given by:

$$I_p \sim |(\chi_e^{(2)})^2 + (\chi_o^{(2)})^2 \pm 2\chi_e^{(2)} \cdot \chi_o^{(2)}| \tag{2.17}$$

where "+" stands for domain A, "-" for domain B. In the conventional approach, where *time-reversal* is the operation mapping domains into each other and dissipation is absent, $\chi_o^{(2)}$ must be purely imaginary and $\chi_e^{(2)}$ purely real (Fig. 22(a)), since then dissipation is necessarily absent. In this traditional approach, the first two components of the sum in eq. (2.17) are real, while the last one is imaginary. Because it is the modulus of the whole sum that determines the output intensity, the domain contrast is lost since

$$|\text{a+ib}| = |\text{a-ib}|, \tag{2.18}$$

[22]This is possible e.g. in antiferromagnets like Cr_2O_3 or those with inequivalent magnetic sites.

which is in odds with experiment [5]. This is not the case if one uses the correct operation of "moment-reversal" for the symmetry classification, since then both tensor elements $\chi_o^{(2)}$ and $\chi_e^{(2)}$ are just complex numbers without any constraints on their relative phase, see Fig. 22b, and domain imaging is possible, as described in [67]. Consequently, the symmetry analysis yields very different predictions if one uses time- or spin-reversal. For the frequencies far from resonances, however, the complex phase difference between $\chi_o^{(2)}$ and $\chi_e^{(2)}$ approaches 90°, and the domain contrast is lost also in the "moment-reversal" description (in agreement with experiment [5]).

Finally we would like to remark on the validity of previous work on the group-theoretical classification of (magneto-)optical tensors. According to Pan *et. al.* [12], the time-reversal operation forces the tensor elements to decouple into mutually exclusive sets of purely real and imaginary ones (if all the kinds of dissipation are neglected). In addition, the crystal symmetry forces the tensor elements to decouple into mutually exclusive sets of elements odd and even in *magnetization*-reversal, these two divisions are equivalent in the absence of conventional dissipation, i.e. real (imaginary) elements are even (odd) in the magnetization. These are the results of a purely quantum-mechanical approach, where the Hamiltonian is Hermitean (non-dissipative). In a real experiment, the laser spot size is much bigger than the Wigner-Seitz cell, thus the experimental response is of macroscopic character. In order to describe this macroscopic response one should not apply uniquely microscopic conclusions to the analysis of these tensor elements. Consequently, taking into account the dissipation in frequency space (i.e. redistribution of the response frequencies) and thus the nature of SHG as a dynamical process (which rules out the applicability of the time-reversal operation) will prevent the classification of tensor elements as real or imaginary ones, although for systems with higher symmetry the classification of tensor elements as odd and even ones in the magnetization (or in the antiferromagnetic order parameter $\mathbf{L}$) can still apply. The nonlinear susceptibility tensor $\chi^{(2\omega)}$ was usually approximated to be real far from resonances. This was justified for the crystals previously mostly used for SHG, and even more extensively as textbook examples [68, 69], which were usually wide-bandgap insulators. This approximation is not valid in the systems described by us: metals and transition metal oxides, where at any frequency one is close enough to one of the resonances (this will be shown in Sec. 3.3). Thus, the only choice for an operation which accounts for the spin structure is "moment reversal", realized as a spatial operation.

Summary of symmetry analysis:

In our symmetry analysis, we took into account all the spin configuration of low index surfaces of fcc antiferromagnets. As the result, we determined

- the nonvanishing elements of the nonlinear optical susceptibility tensor
- the behavior of those tensor elements in domain operations (domain-parity)

Knowing these results we can state that

- SHG is able to detect the surface antiferromagnetism
- distinguish it from any other magnetic phase
- the particular spin structure at the surface can be detected by SHG in many cases
- domain imaging of antiferromagnetic surfaces can be performed experimentally

These interesting results of our symmetry analysis do not complete our work on SHG from antiferromagnets. So far we cannot say anything about the magnitude nor complex phase of the nonvanishing tensor elements. Their frequency dependence (spectrum) remains uncovered as well. In order to solve these problems, we need an electronic calculation. For the purposes of achieving our ultimate goal, which is the description of the dynamics of SHG, we also need an electronic many-body theory. This theory will be presented in the next chapter of this thesis.